A review on sustainable production of graphene and related life cycle assessment

2D Materials

TOPICAL REVIEW

A review on sustainable production of graphene and related life cycle assessment

J Munuera[1,*], L Britnell[2], C Santoro[3], R Cuéllar-Franca[4] and C Casiraghi[1,*]

[1] Department of Chemistry, University of Manchester, Manchester, United Kingdom
[2] Graphene Engineering Innovation Center, University of Manchester, Manchester, United Kingdom
[3] Department of Materials Science, University of Milano-Bicocca, Via Cozzi 5, 20125 Milano, Italy
[4] Department of Chemical Engineering and Analytical Science, University of Manchester, Manchester, United Kingdom
* Authors to whom any correspondence should be addressed.

E-mail: munueraj@tcd.ie **and** cinzia.casiraghi@manchester.ac.uk

Keywords: graphene, sustainability, life cycle assessment, 2D materials

OPEN ACCESS

RECEIVED
26 June 2021

REVISED
23 October 2021

ACCEPTED FOR PUBLICATION
1 December 2021

PUBLISHED
28 December 2021

Abstract

Advanced materials such as graphene and the family of two-dimensional crystals are very attractive because of the myriad of applications that could be developed based on their outstanding properties. However, as soon as material development reaches enough maturity for production to be scaled up and to enter the market within products, it is crucial to place the technology in the context of possible risks to economic well-being, social equity and environmental harm. This review aims at highlighting the current state of art on sustainable development of graphene-related materials and related environmental impact assessment studies using life cycle assessment (LCA). We show that sustainable development has focused mostly on the use of waste or low cost materials as precursors. However, the findings from relevant LCA studies reveals the limits of this approach, which does not take into account that waste recycling is often very energy intensive. We provide an overview on the life cycle environmental impact assessment, with a focus on global warming potential and energy demand, carried out on different graphene productions methods for specific applications, ranging from composites to electronics. Finally, an outlook is given focussing on the comparison of the different production routes and the results from the LCA.

1. Introduction

Sustainability is becoming a very important aspect in manufacturing because of the growing concerns over its environmental impact. Considering the complexity and energy demanding preparation and processing routes of advanced materials, evaluations on their environmental impact are of crucial importance. For example, plastics is one of the most commonly used material due to its wide range of tuneable physicochemical properties, low weight, resistance to acids, and low-cost production. Yet, the exponential use of plastics with related increase in their waste, and low value recycling, has led us to face new challenges in material science, associated to generation of microplastics and nanoplastics. There is growing evidence that humans are exposed to such micro- and nanoplastics through inhalation or ingestion and that the small size of these particles may allow for bioaccumulation and retention in the body [1–3]. Hence, it is very important to discuss sustainable development of advanced materials already at the early stages of their commercial exploitation.

One of the most recent advanced materials with large potential in a wide range of applications is graphene [4], defined as a single layer of graphite. The development of several production methods as well as the ability to easily tune the surface properties via covalent and non-covalent methods has led to the production of a large family of graphene-related materials (GRMs), figure 1. The ability to produce different graphene grades is very useful for developing applications as each grade will match with the material's requirements for a specific application [5]. The 'graphene roadmap' has envisaged the use of GRMs in many different fields, ranging from electronics, photonics, sensing to composites, energy storage devices and bioapplications [6]. In this framework, some of the GRMs applications are still at the very early stages,

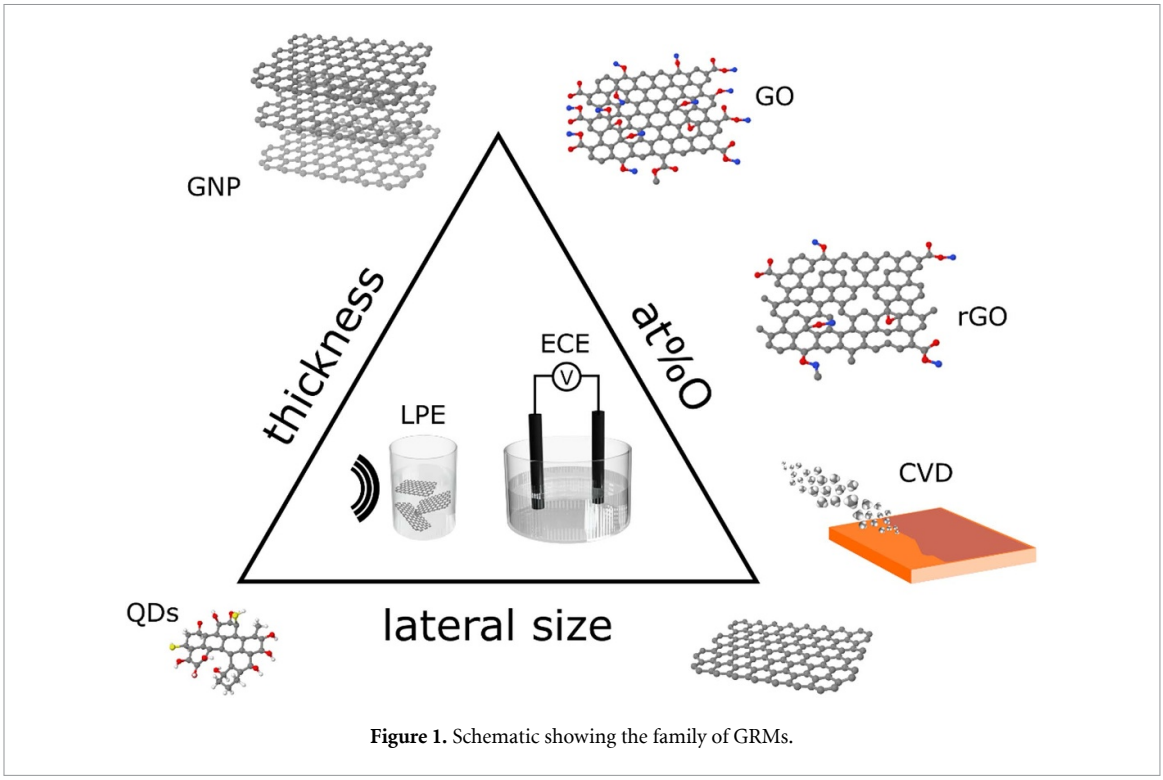

Figure 1. Schematic showing the family of GRMs.

while others have already developed products on the market.

To a first approximation, the scale of any GRM-related sustainability issues should be proportional to the scale of global production volume. It is accepted that in nascent markets there is a high degree of uncertainty in market forecasts, as highlighted by Döscher *et al* [7]. Market forecasts are prone to significant errors (both over and underestimating supply) due to the small market volume, disproportionate impact of new players, a lack of trend data and inaccurate assumptions. Thus, forecasting the scale of future environmental impact is equally prone to uncertainty. However, it is to note that graphene production has been growing rapidly for several years with remarkable recent announcements from Nanoxplore (4000 t a^{-1} coming online in 2020) [8] and Sixth Element (1000 t a^{-1}) [9]. In 2021, the reported production capacity across the top 34 suppliers totals 9.7 kT in 2021 and estimates of the demand are ∼900 tonnes. Composites (275 tonnes) and batteries additives (160 tonnes) make up ∼50% of the orders. Combined with the demand from paints & coatings, electronics, automotive and construction sectors this accounts for 75% of the total market demand [10]. While this is far below the reported global production capacity (>10 kt a^{-1} in 2020) [7], many large usage product streams are ready to come online making a review of the associated sustainability a timely subject of merit.

Despite the strong potential of GRMs in future applications and the ability to mass produce low grade graphene at a low cost, very little attention has been dedicated so far to potential environmental impacts of their production and manufacturing. Several review articles discussing the preparation of GRMs using non-conventional starting materials have been published [11–14]. Different approaches, with common starting materials but making use of environmentally friendly reagents and processes have been recently described in numerous works [15–22]. However, many works have mostly focused on the use of waste material as a source for GRMs, but other aspects related to manufacturing and disposal, including recyclability, have hardly been considered.

The goal of this review is to offer a comprehensive and critical look on the sustainable production of GRMs as well as a prospective view about the future of this kind of strategies and their results, by considering also their life cycle environmental impacts using life cycle assessment (LCA). LCA is an environmental management tool that quantifies the environmental sustainability of products, processes or activities throughout their life cycle [23, 24]. This is achieved through the quantification and translation of environmental burdens into potential impacts, e.g. greenhouse gases emissions into global warming potential (GWP) [23], using scientific models developed by international organisation such as the Intergovernmental Panel on Climate Change (IPCC) and the World Meteorological Organization (WMO) [25]. Typical life cycle stages considered in LCA include the extraction and processing of raw materials, manufacture, use, end-of-life management, e.g. reuse, recycling, final disposal, and transportation across the stages.

This review is organized as follows: in the first part, we will provide an introduction to GRMs and

their traditional production routes and characterization methods as well as a short introduction on LCA. In the second part, we will give an overview of the works published in the contest of the sustainable production and related LCA. In the last part of the review, we provide an outlook on the use of waste materials for production of GRMs by highlighting the most promising waste materials and processes, taking into account the preparation procedures, yield and quality of the final products.

1.1. Graphene-related materials

The GRMs family encompasses a wide variety of materials ranging in thickness, lateral size, chemical composition, structural defects and chemical moieties, which all determine the properties of each GRM, figure 1. Common examples are graphene (single to multilayer), graphene oxide (GO), reduced GO (rGO), quantum dots (graphene or GO) and graphene-like carbons.

The layer number of GRMs indicates the number of graphitic layers comprising each material, and they are often described as mono-/single, few- and multi-layer, generally corresponding to one, less than ten and more than ten layers respectively. In terms of lateral dimensions, GRMs below 10 nm are classified as quantum dots, referred to as graphene quantum dots (GQDs), GO quantum dots (GOQDs) or carbon quantum dots (CQDs), depending on their chemical structure [6, 26–30]. Note the nomenclature QDs denote a 0-Dimensional material, which therefore will have different properties compared to two-dimensional (2D) graphene, although made by the same type of carbon bonding. Dimensionality is indeed well known to affect the optical and electronic properties of nanomaterials. Larger GRMs (ranging from tens of nm to μm-sized) are often described as platelets, sheets, flakes among other terms, and often with the prefix nano-, indicating their small size in the range [6, 26–30]. Although standardised terminology of graphene and 2D materials has been published [31], there remains no current consensus on the precise meaning of these terms, and thus it is fairly common to see them used interchangeably in different works. In regard to their chemical structure, GRMs are usually labelled as graphene or GO when their oxygen content is close to 0 and 50 at.% respectively, but again it is not uncommon to read descriptions of highly oxidised GRMs labelled as graphene, and vice-versa [6, 26–30]. Lastly, there is a number of GRMs with an array of 3D morphological characteristics, comprising graphene foams, graphene-like carbons, carbon nanosheets among other terms [6, 26–30]. We finally remark that in some applications, such as in the biomedical field, the surface charge is also another parameter to take into account to define the GRM's properties [32, 33]. It is well known that cationic nanomaterials show better interactions with the biological environment, such as better cellular internalisation due to stronger affinity to the negatively charged biomaterials such as small interfering ribonucleic acid [34]. Furthermore, the charge is also a significant contributor to the nanomaterial's toxicity [35].

1.2. Graphene-related materials preparation methods

Preparation methods of GRMs have been widely discussed in a number of reviews, [6, 26–30] and are often divided between *top-down* and *bottom-up* strategies. The former is based on the delamination of graphite down to multi-, few- or monolayer sheets, while the latter consists on the assembly of molecular or atomic precursors to obtain graphene. Currently, the most widely spread *top-down* preparation methods for GRMs are: the Hummers' method [36], the liquid phase exfoliation (LPE), [37–39] and the electrochemical exfoliation (ECE) [40–44]. The Hummers' method relies on the use of strong oxidants on graphite, promoting the formation of oxygen-containing functional groups that expand the interlayer distance and facilitate the dispersion of GO monolayers in water or other solvents. GO shares certain morphological characteristics with graphene, but owing to the covalent functionalization caused by the oxidation step, its mechanical, electrical, electrochemical and optical properties are substantially different from those of pristine graphene. A number of modifications and improvements to the original method have been reported [45–47], as well as reduction processes, giving rise to rGO [48, 49]. rGO is still a defective graphene as the reduction process typically introduces new defects, while removing oxygen from the carbon scaffold, but in term of electronic grade, rGO is conductive and therefore can be used as electrode [50]. In LPE, stable colloidal graphene dispersions are obtained through the exfoliation of graphite into few-layer nanosheets [26, 39, 51, 52]. Exfoliation is achieved by means of sonication [39], shear mixing [53], microfluidization [54] or ball-milling [55], and either organic solvents or surfactants are needed for the colloidal stabilization of graphene. The GRM obtained by LPE is characterized by a distribution in size (from 800 to 50 nm) and in thickness (from 1 to 100s of layers) [26]. The exact lateral size and thickness distribution can be tuned by liquid cascade centrifugation [56]. The graphene material obtained keeps its pristine structure, i.e. no significant increase in their oxidation or defects has been observed, unless harsh sonication conditions are used [57, 58]. The (anodic) ECE is a method driven by electrical current, based on the intercalation of ions from an aqueous electrolyte into a graphite electrode [40, 41]. The intercalation is driven by an applied voltage, which also promotes the decomposition of the electrolyte into gas species, contributing to the expansion of graphite, and its subsequent exfoliation into graphene nanosheets. The resulting material is comprised of

mono- to few-layer graphene, with lateral dimensions in the range of few μm [40, 41]. Depending on the chemical reactions induced by the electrical current, the obtained graphene can be oxidised and defective, or can be similar to pristine graphene [59, 60].

The starting materials are often based on commercially available graphitic materials and usually, inexpensive e.g. graphite powder in Hummers' method and LPE, graphite rods and foil for ECE. Most preparation methods are not generally considered as environmentally friendly, owing to the use of hazardous reagents, solvents and/or processes [6, 26–30]. With the dual intent of reusing waste materials and reducing the need for pure, high-quality starting materials, numerous research groups have developed strategies to produce GRMs from carbon-containing waste products. This research is extensively covered in the first part of this review.

Bottom-up methods, such as chemical vapour deposition (CVD) and epitaxial growth, have been covered elsewhere [12, 14], but they will be discussed and compared to top-down methods in the third part of this review, dedicated to LCA.

1.3. Characterization of GRMs

When considering the preparation of GRMs using waste materials as carbon sources, one of the main questions to address is related to the quality of the final product in terms of chemical and morphological features, such as composition, defects, layer number, lateral size, conductivity, etc. These parameters must be evaluated and compared with those of GRMs prepared by common procedures.

Unfortunately, characterization of GRMs is very challenging, in particular when produced by LPE and ECE. The first measurement standards have been only recently established within ISO/TC 229 [31]. Typically, a large range of techniques are used to provide complementary information, and they have been extensively described in several recent reviews [6, 26, 61–63]. Here, we only provide a short list of the techniques that are typically used to characterize GRMs made by waste materials as precursors. Scanning and transmission electron microscopy techniques (SEM and TEM, respectively) are very powerful techniques to study GRMs morphology, and can help elucidate lateral sizes and number of layers [64]. In the case of liquid dispersions of GRMs, atomic force microscopy (AFM) provides information on flake thickness and lateral size [26], although determination of number of layers could be more challenging for solution processed GRMs [65]. The chemical composition can be determined by means of different techniques, e.g. elemental analysis, energy-dispersive x-ray spectroscopy (EDS, EDX, EDAX), inductively coupled plasma atomic emission spectroscopy, x-ray photoelectronic spectroscopy (XPS), each one with its own limits, in terms of applicability [6, 26, 27]. Given the crystalline and layered nature of GRMs, diffraction techniques are often used for their characterization, e.g. x-ray diffraction (XRD), selected area electron diffraction [6, 26, 27]. A number of spectroscopic techniques are often used to characterize different parameters of GRMs. In particular, Raman spectroscopy has proven to be one of the most powerful techniques for the characterization of GRMs [66–68]; although a unified method to extract the thickness of all types of GRMs is still missing, the intensity ratio of the D and G band (I_D/I_G) is often used as key parameter to evaluate the amount of defects in GRMs [69, 70]. Note that this parameter alone may be misleading as I_D/I_G does not always increase with the number of defects, in particular at very high defects concentration, and it also changes with the laser excitation energy [69, 70]. Furthermore, in case of defective GRMs, Raman spectroscopy cannot be used to determine the thickness by using the shape of the 2D peak [71]. Fourier transform infrared spectroscopy (FTIR) allows the identification of functional groups, while ultraviolet–visible–near infrared spectroscopy provides information on the electronic conjugation and oxidation on GRMs [6, 26, 27]. Some GRMs (e.g. QDs) exhibit photoluminescence (PL), as this property is related to their size and chemistry [72, 73]. Zeta-potential analysis and dynamic light scattering are used to measure the charge and hydrodynamic size of particles in colloidal dispersions, respectively, and therefore provide information about the colloidal stability [6, 26, 27]. Thermogravimetric analysis (TGA) is used to study the thermal stability of GRMs and to get information on the presence and amount of functional groups, as they get removed at different temperatures [48]. Nitrogen adsorption isotherms and their analysis through the Brunauer–Emmett–Teller theory (BET) provides information about pore size distribution and specific surface area, respectively [74]. Electrical conductivity measurements are used to study the electronic properties of GRMs, which in turn depend on structure, size, thickness and surface chemistry of the flakes [6, 26, 27].

1.4. Introduction to LCA

LCA is widely used in industry, Academia and governments for a variety of applications as its results can be used to make informed decisions across various issues [23, 24]. Some examples include product development, process design optimisation, comparison and selection of more environmentally sustainable alternatives and policy making [23]. However, LCA only addresses the environmental dimension of sustainability [24] and in order to conduct a sustainability assessment, LCA must be integrated with other complementing tools capable of addressing the economic and social dimensions of sustainability, such as life cycle costing and social LCA [75].

The LCA methodology is a standardised environmental assessment tool recognised under the

ISO environmental management 14040 series, which comprises of international standards and technical reports [23, 24]. The principles and framework, and the requirements and guidelines are outlined in the ISO 14040:2006 [76] and ISO 14044:2006 [77] standards, respectively. According to these guidelines, the LCA methodology comprises four iterative stages: (a) goal and scope definition; (b) inventory analysis; (c) impact assessment; and (d) interpretation. These will be discussed briefly in the next sections. The LCA, being a complex methodology, has its own limitations [78]. For example, the outcome of any LCA study will be highly dependent on data availability and reliability, e.g. representative of the system. The implementation of the methodology can be time consuming/resource intensive and the interpretation of the results requires specialist knowledge, impartial judgement and transparent communication, e.g. reporting of assumptions made. Some of the LCA requirements (as defined in the ISO standardised framework) are open to interpretation, therefore adding to this complexity when it comes to addressing multifunctionality issues in a system or defining consistent functional units and system boundaries for a given sector or application. This is particularly the case when it comes to applying the LCA methodology to emerging technologies and materials, where a consensus among experts may be required for setting more specific guidelines, e.g. predefined assumptions or reporting guidance. The carbon capture and utilisation (CCU) community, for instance, has recently developed specific guidelines in order to improve comparability of LCA studies of CCU [79, 80] and support decision-making across stakeholders.

The next sections discuss each of the four stages in LCA as dictated in the ISO 14040 and 14044 guidelines, making emphasis on the mandatory elements of LCA and reporting of results, and the purpose of optional elements such as normalisation and weighting. A comprehensive description of each one of the LCA phases and their elements can be found in Hauschild *et al* [81] and the ISO 14040 and 14044 standards [76, 77].

1.4.1. Goal and scope definition

The first step in the LCA methodology consists of defining the reasons for carrying out the study, the intended application and intended audience, thus setting the context of the study and the subsequent steps [23, 24, 77, 81]. This is followed by the scope definition, where the system under study is defined and the function it delivers is established, which leads to the selection of the system boundaries and the functional unit of the study [24]. The interpretation of the results and overall outcome of an LCA study will be directly influenced by the choices made during this initial step, hence its importance.

When taking a life cycle approach, the contributions from some or all the different stages in the life cycle of a process, product or activity are accounted for, including the extraction of raw materials, manufacturing or processing stages, use or application, recycling and/or reuse of materials, end-of-life, and transportation. Typical system boundaries can be studied from 'cradle to gate', 'cradle to grave' or 'gate to gate', which only considers activities within the manufacturing stage. Choosing the functional unit of the study is no trivial task and it will depend on the goal of the study. For example, when comparing two types of packaging material, these should be compared in terms of their function, i.e. to 'contain' a product, rather than their physical quantities, e.g. per *kg* of material, as different amounts of materials may be required to provide the same function due to materials' density differences [81].

1.4.2. Inventory analysis

The second phase consists in the quantification of all the inputs, e.g. raw materials, energy, and outputs, e.g. products, co-products, waste, of the system under study and associated emissions, i.e. air, water and soil, also known as the life cycle inventory (LCI) of the system [23, 77]. Depending on the nature of the study, data can be obtained from various sources. This may include data directly provided by industry, e.g. commissioned study [23], sourced from literature, process simulation data, scaled up experimental data, databases, expert calculations, etc. In the absence of data, approximations and/or informed assumptions can be made. However, the reliability of the results of an LCA study will largely depend on the quality of the data and soundness of the assumptions made [23, 24].

The representativeness of the data is another important factor to consider in LCA, as the quality level will depend on the geographical, time-related and technological representativeness of the data used [81]. The quality and uncertainty of the LCI data can be assessed using a variety of methods including data quality ratings [82], consistency checks (ISO), and other analytical methods such as pedigree matrix or Monte Carlo analysis [81]. LCA practitioners heavily rely in the use of LCA databases for sourcing data [23], e.g. Ecoinvent database [83], as these databases already include LCI data for a wide range of industrial processes, manufacture of basic chemicals (organic and inorganic) and other raw materials, energy production and transportation systems, waste management processes, etc. These databases include elementary flows as well as the emissions released.

1.4.3. Impact assessment

This phase, also known as life cycle impact assessment (LCIA) consists of translating the environmental emissions resulting from the inventory analysis phase into environmental impacts [23, 24]. This is carried out through the selection of impact categories, classification of environmental burdens and their characterization, which are referred to as the

'mandatory' steps in LCIA [77]. The selection of environmental impact categories must be consistent with the goal and scope of the study [23, 81]; in some cases ones will become more relevant than others due to the sector's or activity's nature. However, when looking at conducting an environmental sustainability assessment, all impact categories must be considered in order to prevent burden-shifting across impacts [81]. Environmental impact categories can be divided into: emission-related impacts, e.g. GWP, acidification potential, human and eco-toxicity potential; and extraction-related impacts, e.g. abiotic depletion of resources potential [81].

Environmental emissions may comprise a wide range of substances, which in turn are responsible for different environmental impacts depending on their known potential effects and their environmental mechanism, e.g. fate, exposure, effects, damage [81]. Therefore, the LCI results must be classified into their corresponding impact categories. For example, carbon dioxide is a well-known greenhouse gas and contributes to global warming, whilst CFCs are known to cause global warming and ozone depletion [84]. Once the environmental burdens are classified, these are translated into environmental impact potentials using characterization factors. These factors are estimated using scientific models developed by international organisations [81], such as the IPCC and the WMO [25]. As a result, each environmental impact category is measured using distinctive equivalent units that take into account the relative effect of all relevant substances with respect to a designated reference [24]. For instance, GWP, which measures the relative impact of greenhouse gases on radiative forcing [85], uses carbon dioxide as the reference substance and has mass units of CO_2 equivalent, e.g. '*kg* of CO_2 equivalent'. The use of characterisation factors, therefore, allow measuring and comparing the radiative forcing effect of other greenhouse gases with respect to carbon dioxide over a given period of time [86]. The characterisation factor of methane for a 100 year time horizon ranges between 28–36 kg of carbon dioxide equivalent per kg of methane [85], and this factor indicates that methane has 28–36 times the cumulative radiative forcing of CO_2 [81].

There is a wide range of LCIA methods available and their selection will depend on various factors such as latest developments in the field, type of assessment, e.g. midpoint or endpoint, compatibility with other studies, and the use of regional normalisation factors [81]. The most commonly used methods include CML [87] and ReCiPe [88], and the ILCD [89] which include European as well as global normalisation factors. In the United States, the Environmental Protection Agency's in–house LCIA method TRACI is strongly recommended due to the use of regional normalisation factors [90]. The LCIA step is commonly carried out using specialised LCA software that includes one or more LCIA methods to choose from. Examples of software packages for LCA includes SimaPro [91] and GaBi [92], which are both commercially available, as well as open sourced ones such as Open LCA [93] and CCaLC [94].

Following the impact characterisation step, other optional steps such as normalisation and weighting can be applied to the results obtained to better understand the meaning of these [24, 81]. For example, normalisation is done to understand the relative magnitude of the results obtained for each indicator, i.e. share of a regional impact [24, 81]. Weighting can help determine the level of importance of the environmental impacts assessed using weighting methods [24, 81, 84]. However, this step tends to lack objectivity as it will reflect the preferences or priorities of the individuals selecting the weighting factors [24, 81].

1.4.4. Interpretation

This phase consists of evaluating the LCI and LCIA results obtained with respect to the study's goal and defined scope, with the purpose of reaching conclusions and/or making recommendations [24, 77, 81]. This is achieved through an iterative process, starting with the identification of significant issues [24] such as major burdens, environmental impacts and major contributors or 'hotspots' in the life cycle [23]. This is followed by an evaluation process to determine the robustness and reliability of the study through completeness and consistency checks as well as sensitivity analysis [24, 81] around the assumptions made, methods employed and data used, e.g. quality and sources [81]. Once the evaluation process in complete, conclusions can be reached and recommendation can be made according to the goal and scope of the study and to the intended audience. It is also important to identify and report the limitations of the study based on data quality and availability, and assumptions made [24, 81]. This is to ensure transparency and impartiality in LCA reporting [23].

2. Graphene-related materials prepared from waste materials

In order to establish preparation protocols of GRMs from carbon containing waste materials, careful consideration needs to be accounted regarding the chemical composition and morphology of the initial precursors. Waste materials containing graphite can be readily exfoliated into GRMs by means of common strategies with little or no previous treatment. However, carbon-containing waste materials are often composed of complex mixtures of chemicals (e.g. biomolecules, polysaccharides, polymers) that need to be transformed into a carbonaceous material. This transformation is generally realised by means of thermal treatments and, depending on the specifics of this step and the desired characteristics of the final GRM, a final exfoliation step is usually needed.

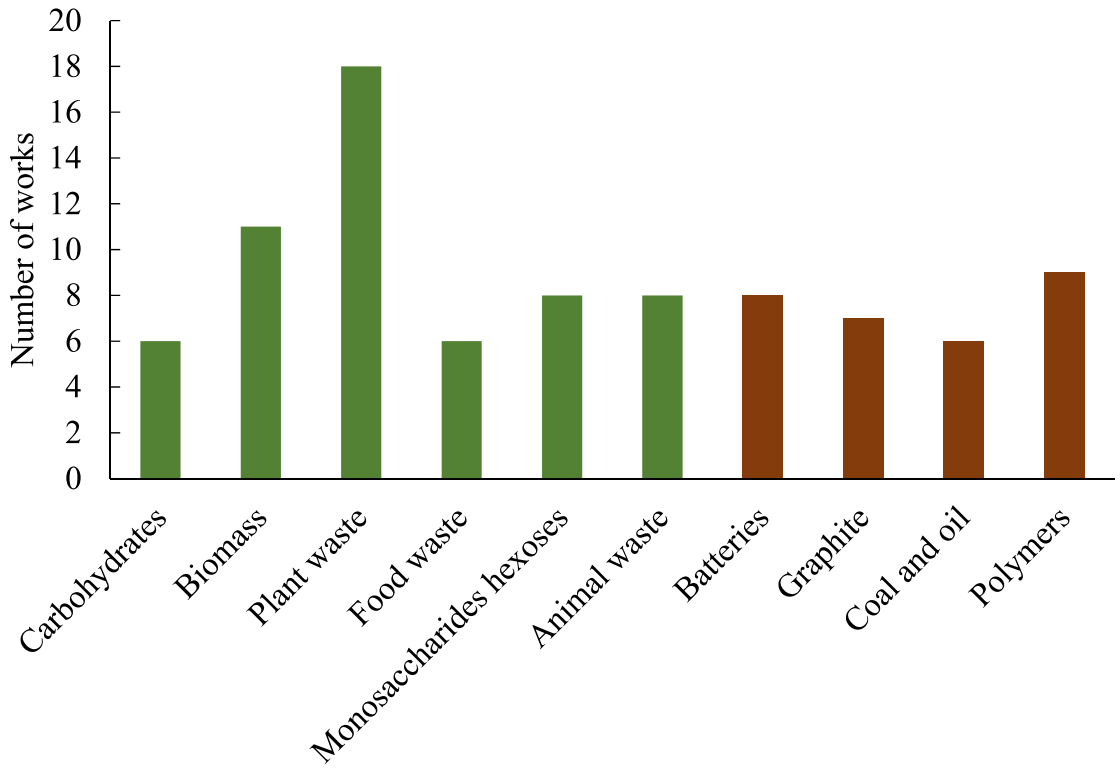

Figure 2. Summary showing the number of works published in the last 10 years reporting the use of carbon-based waste (biological in green; non-biological in red) to produce GRMs.

Based on the current state of the art on use of carbon containing waste materials for the preparation of GRMs, in this review the carbon sources have been classified into two broad categories: (a) biological waste and (b) non-biological waste, as shown in figure 2. The selection was made based on the number of works published in the last 10 years as well as the chemical nature of the source, since this strongly affects the preparation methodologies. We have found a total of 88 works, of which 66% are related to biological sources. Each category can be divided into different sections attending to the specific waste material (i.e. paper, wood, plants, animal, batteries, graphite, coal, polymers), as displayed in figure 2 and tables 1–10. These categories are not intended to be exhaustive, since a number of works describe the use of more than one type of waste material, but they are meant to provide a broad understanding of the current progress on the use of each kind of waste in terms of preparation strategies and results.

2.1. Biological sources

2.1.1. Carbohydrates and polysaccharides

Carbon-containing wastes from biological sources are currently used as the main initial precursor for the sustainable production of GRMs, as summarized in table 1. A wide variety of materials have proven to be suitable to this purpose, such as paper, wood, sugar and chitosan. Since the composition of these carbon sources comprises non-graphitic materials (e.g. carbohydrates, polysaccharides), a graphitization process is required in order to transform the crystal structure [95–97]. This goal is usually attained by means of thermal treatments (pyrolysis) at temperatures ranging from a few hundred to above 1000 °C and often in the presence of catalysts or with the aid of intermediate phases. The chemical transformation due to the thermal treatment is optimized in inert (N_2 or Ar) or slightly reducing (mixture N_2 and H_2 or N_2 and NH_3) controlled atmosphere avoiding the presence of oxygen that might led to combustion and formation of highly oxidized material, volatile compounds and gases decreasing the desired product yield. The graphitization mechanism for materials such as cellulose [95, 96] and wood [97] has been studied outside the preparation of GRMs, but some of the works presented here provide insights on the effects of temperature and catalysts. This process often involves the condensation of organic molecules (i.e. polysaccharides in the case of cellulose) into an intermediate phase at temperatures in the range of few hundreds of °C. This phase is then treated at temperatures up to 1000 °C (often in the presence of a catalyst), which promotes the transformation into a graphitic structure.

The first report, to the best of our knowledge, on the use of paper for the preparation of GRMs is the work of Zhao *et al* in 2013 [98]. Paper cups were first treated with KOH and impregnated with Fe^{2+} ions, and subsequently heated to 1100 °C in inert N_2 atmosphere, figure 3. This treatment promotes the transformation of lignin and hemicellulose fibres

Table 1. Starting materials, preparation steps and characterization of GRMs produced from carbohydrates and polysaccharides.

Precursor	Pre-treatment	Treatment/exfoliation	Product	Microscopy	Elemental analysis	Diffraction	Spectroscopy	BET ($m^2\ g^{-1}$)	Yield	References
Paper cups	1 M KOH, 72 h;1 M $(NH_4)_2FeSO_4$, 48 h, N_2	1100 °C, 45 min, N_2	Graphene sheets	Few to multilayers ~1 μm lateral size		Peaks at 26.2º, 42.5º, 54.4º, 77.4º	**Raman**: D, G, 2D peaks Abs peak at 275 nm			[98]
Paper	H_2SO_4, 160 °C, 2 h	HNO_3, 45 °C 30 min sonication	GOQDs	Wrinkled 0.5 nm thick, ~15 nm lateral size	C/O = 2.0	Peak at 23º	**FTIR**: C–OH, C=O, C–O, C=C, C–O–C, C–H, COOH Abs at 200, 320 nm. Fluorescence			[99]
Paper	HCl, 72 h; 1350 °C, 3 h, Ar	Cobalt(II)acetate, 1,10-phenanthroline, 800 °C–950 °C, 1–2 h, Ar	Co/graphene, Co_3O_4/graphene	50–200 nm particles pores formation	C/O = 16–21.5	Peaks at 23.5º–26.3º	I_D/I_G = 1.20–1.51	542	10%–20%	[100]
Paper	Cover with urea	1000 °C, 2 h, N_2	Graphenedecorated carbon paper	Graphene sheets			**Raman**: D, G, 2D peaks	63.4	36%–50%	[101]
Paper	Cover with urea	850 °C, 2 h, N_2	Graphene	Fibrous morphology	45.50%–60.36% C, 0–15.16% O, 20%–36% N Impurities: Mg, Al, Si, Cl, Ca, Fe, <3% each	Broad peak at 26.5º		63.4		[102]
Cellulose	Water, 200 °C, 12 h	1000 °C–1500 °C, 1 h, N_2	CQDs	Graphitic and amorphous domains	90.8%–92.2% C, 7.8%–9.2% O	Broad peaks at ~24º, 44º	I_D/I_G = 1.30–1.67	5–12		[103]

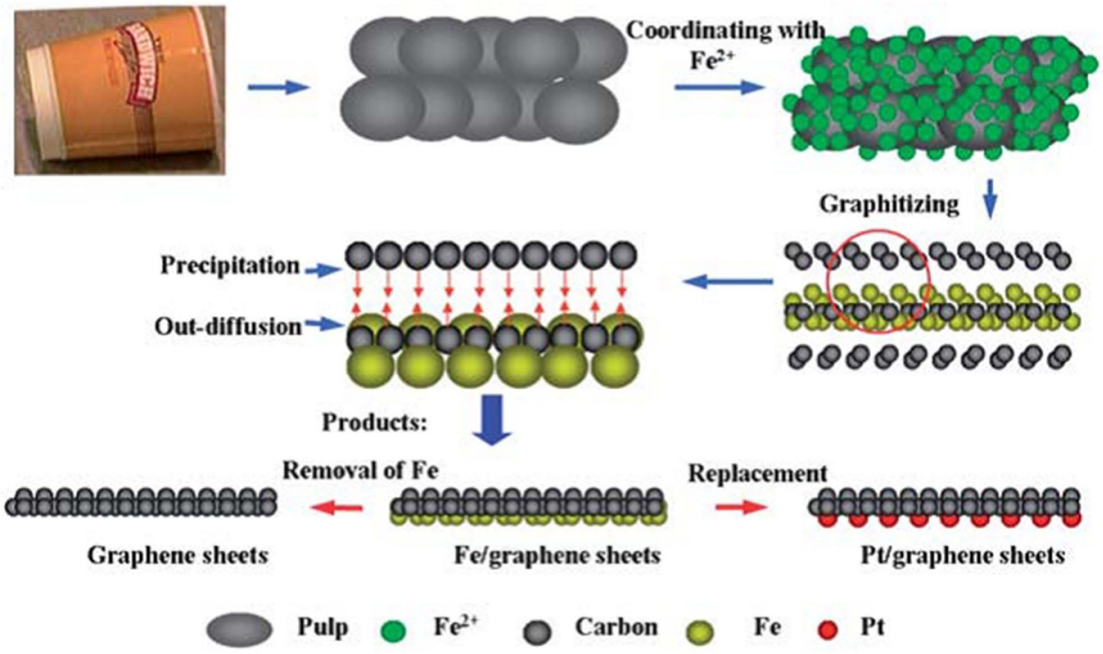

Figure 3. Fe-catalysed preparation of graphene from paper cups. Reproduced from [98] with permission of The Royal Society of Chemistry.

present in the paper into multilayer graphene, in a process mediated by the formation and decomposition of Fe_3C. The resulting material is functionalized with Fe nanoparticles (NPs), which can be removed to obtain non functionalized graphene, or replaced with Pt NPs by means of an interchange reaction. A different approach was taken by Adolfsson *et al*, who treated paper with H_2SO_4 and HNO_3 in two separate steps at low temperatures, by obtaining GOQDs [99]. The acid treatment transforms the fibre structure in the paper into small (0.5 nm thick and 15 nm lateral size) GOQDs, whose fluorescence was also measured, showing an emission peak at 450 nm. Co and Co_3O_4 functionalized graphene structures were obtained by Xu and co-workers from paper waste [100]. The paper was first treated with HCl and subsequently subjected to thermal treatment at 1350 °C in argon atmosphere to obtain a microporous carbonaceous pulp, which was then mixed with cobalt acetate and phenantroline and heated up to 800 or 950 °C to yield Co_3O_4 and Co/graphene respectively. Another strategy for the conversion of paper into graphene materials relies in the use of urea as a reagent, as it promotes the formation of an intermediate g-C_3N_4 phase that will evolve to graphene. Moreover, urea is beneficial in the process because it can be used as nitrogen source for obtaining carbonaceous materials containing nitrogen functionalities and as templating agent, as its sublimation leads to the creation of voids increasing the available surface area. Both the works of Ye *et al* [101] and Singu *et al* [102] made use of this method, applying temperatures of 850 °C–1000 °C after mixing paper waste with urea. Their results show the formation of GRMs with varied amounts of oxygen and nitrogen, as well as a range of impurities, depending on the exact paper source. Pure cellulose was used by Xie *et al* to prepare CQDs through a two-step process [103]. An aqueous solution of cellulose was first heated in an autoclave at 200 °C, and the resulting solid was carbonized at 100 °C–1500 °C in a N_2 atmosphere. As a result, CQDs with 7.8–9.2 at.% oxygen content, and graphitic and amorphous domains were obtained. SEM and TEM imaging of the products show the presence of small particles, but precise size measurements were not provided.

Table 1 shows that amongst the few works based on paper-based waste as precursors, only two groups have reported graphene nanosheets, [98, 101] but quantitative elemental composition is lacking in both cases.

2.1.2. Waste biomass

A variety of other waste biomasses (i.e. wood, leaves, bagasse, fruit, paper, bones, cow dung, industrial soot) was used by Akhavan *et al* to obtain GO [104]. The starting materials were first heated up at 400 °C–500 °C, then treated with $FeCl_3$, and subsequently used as a graphite substitute in a modified Hummers' method. The resulting GO is made of mono- and few-layer nanosheets, showing contamination of a number of elements in different proportions for each starting material (i.e. N, Na, Mg, P, S, K, Ca, De, Cu, Zn, Pb, <3 at.% each). A very different approach was taken by Chyan *et al*, who used a pulsed CO_2 laser to turn a number of starting materials (e.g. cloth, paper, food, wood) into GRMs [105]. TEM imaging of the products revealed the formation of few-layer graphene sheets with different

chemical compositions, depending on the starting material (50–80 at.% C, 20–40 at.% O, 0–5 at.% N, 0–5 at.% P). Kraft lignin was also recently used in a modified Hummers' process by Li and co-workers to obtain GO [106]. In order to achieve a graphitic structure that could be oxidised and exfoliated, the authors used $Fe(NO_3)_3$ as a catalyst for the graphitization of lignin at 1100 °C in argon and methane atmosphere. Their resulting graphitized samples were used in a modified Hummers' method, yielding GO comprised of 1–3 nm thick flakes. Medium density fibreboard, a wood-derived product, was successfully transformed into a porous graphene-like carbon by Gomez-Martin *et al*, through its nickel-catalysed graphitization [107]. To this end, the starting material was impregnated with $Ni(NO_3)_2$ and heated up to temperatures from 300 to 1000 °C in a N_2 atmosphere, resulting in graphitized and crumpled nanosheets. The latter has an oxygen content of 11–29 at.%, as well as small quantities of nitrogen (2–7 at.%) and residual amounts of nickel (<1 at.%). In a catalyst-free process, spruce tree bark was converted into vertically aligned graphene nanosheet arrays by Sun and co-workers [108]. The bark was ground and mixed with KOH, and subsequently heated up in a N_2 atmosphere at 800 °C–1000 °C. This process yielded nanosheet arrays with high surface area (2028–2385 m^2g^{-1}) and oxygen contents of ∼5–13 at.%. Several research groups have made use of coconut shells as starting materials for the preparation of GRMs. For example, Sun *et al* mixed the shells with $FeCl_3$ and $ZnCl_2$ (acting as catalyst and activating agent, respectively), and then treated the mixture at 900 °C in N_2 atmosphere [109]. This process yielded few- and multilayer nanosheets with low amounts of oxygen and defects (O/C = 0.05812, I_D/I_G = 0.25), as well as a high surface area of 1874 m^2g^{-1}. By using bamboo tinder waste in a multi-step acid and heating treatment, Tade *et al* recently reported the preparation of GQDs [110]. First, the waste material was subsequently treated with HNO_3 and $KClO_3$, followed by a reaction with H_2SO_4 and the heating to 180 °C for 8 h. As a result of this process, 9.8 nm-sized GQDs were obtained. The water dispersible GQDs resulted substantially oxidated (56.9 at.% O), and they showed fluorescence emission peaks at 245 and 365 nm. The works of Darminto *et al* and Asih *et al* made use of the same process and also using coconut shells to prepare rGO [111, 112]. For this purpose, the shells were burned, ground to fine powder, and subsequently treated at 400 °C–1000 °C in air and sonicated in water, yielding materials with layered structure and oxygen functional groups, as evidenced by XRD and FTIR, respectively. Recently, Tamilselvi and co-workers described the use of coconut shells and coir using a much lower temperature catalytic process, mixing the starting material with ferrocene and treating it at 300 °C in air [113]. As a result of this process, few-layer, oxidised nanosheets were obtained. Using a more complex process, Yadav *et al* reported the preparation of porous GO, and its S- or N-doping [114]. The process involves two heating steps (1 h at 300 °C and then 3 h at 750 °C in Ar) in the presence of KOH, followed by two acid treatments (HCl for 12 h and HNO_3 for 12 h). In order to dope this porous GO with S- or N-containing functionalities, the material was mixed with either sulphur or urea, and heated first to 450 °C for 40 min in Ar, and then to 750 °C for 30 min in H_2. The resulting materials (GO, S–GO, N–GO) resulted to be thin (0.9–4.2 nm thick) and porous nanosheet structures as observed by AFM, SEM and TEM. XPS analysis shows C, O, S and N signals, with C content in the 67–85 at.% range, S, N contents of 0.9 and 3.9 at.% respectively and oxygen making up the rest of the composition.

Table 2 shows that this approach is mostly suitable for the production of various forms of defective GRMs.

2.1.3. Plant-derived waste

Biomass organic waste derived from plants has also been successfully processed into GRMs by means of different combinations of chemical and thermal treatments. Palm tree residues (i.e. kernel shell, leaves, empty fruit bunch) were carbonized at 400 °C–900 °C in N_2 atmosphere and subsequently used in an improved Hummers' process by Nasir *et al* obtaining GO as final product [115]. The resulting material was obtained with a 26–37 at.% yield and displayed a porous layered structure and oxygen functionalities derived from the initial oxygen contained in the starting materials. In a later work, palm kernel shells were also used by Nurdin *et al* to prepare GRMs [116]. The shells were first mixed with urea, $FeCl_3$ and $ZnCl_2$, and subsequently heated to 350 °C for 1 h and then to 900 °C for 90 min, all in N_2 atmosphere. The resulting material was comprised of highly graphitized few-layer nanosheets, and while the nitrogen functional groups appear in the FTIR spectra, the detailed composition is not reported in this work. In 2012, Ray and co-workers reported the high-temperature, controlled atmosphere treatment of flower petals [117]. The authors treated the starting materials at 800 °C–1600 °C in Ar atmosphere obtaining thin graphene layers with very low amounts of oxygen (C/O = 82–142) and different amounts of defects (I_D/I_G = 0.37–1.31). More recently, Lu *et al* reported the use of camellia shells for the preparation of a graphene-like nanocarbon [118]. Their process makes use of activation with KOH at 180 °C, followed by a calcination step at 800 °C in Ar atmosphere. The resulting material is made of thin, graphene-like sheets; its characterization revealed the presence of residual nitrogen (<1 at.%) and a surface area of 633–1020 m^2g^{-1}. Another plant-derived waste used for the preparation of GRMs is sugarcane bagasse, which has been the subject of recent works, as listed

Table 2. Starting materials, preparation steps and characterization of GRMs produced from waste biomass.

Precursor	Pre-treatment	Treatment/exfoliation	Product	Microscopy	Elemental analysis	Diffraction	Spectroscopy	BET ($m^2\ g^{-1}$)	Yield	References
Wood, leafs, bagasse, fruit, paper, bones, cow dung, industrial soot.	400 °C–500 °C, 5 d; grinding, 450 °C, 24 h; $FeCl_3$, 60 °C, 1 h	Modified Hummers'	GO	1–4 layers 1 μm lateral size	Impurities: N, Na, Mg, P, S, K, Ca, De, Cu, Zn, Pb, <3% each		$I_D/I_G = 0.9$-1-2			[104]
Cloth, paper, food, wood.	—	CO_2 pulsed laser	Graphene	Few-layers	50%–80% C, 20%–40% O, 0%–5% N, 0%–5% P		$I_D/I_G = 0.2$–1.3		1.2%–7.2%	[105]
Kraft lignin	$Fe(NO_3)_3$, 1100 °C, 1 h, Ar, CH_4	Modified Hummers'	GO	Nanosheets 1–3 nm (1–3 layers) <1 μm lateral size		Peak at 25.6º	$I_D/I_G = 1.1$–1.2 **FTIR**: O–H, C=O, C=C, O–C–O, C–O			[106]
Medium-density fiber-board	Impregnation with $Ni(NO_3)_2$, drying	300 °C–1000 °C, 30 min, N_2	Porous graphene-like carbon	Crumpled graphene-like nanosheets	63%–86% C, 11%–29% O, 0%–1% Ni, 2%–7% N, C/O= 2.2–7.8	Peaks at 26º and 44º	$I_G/I_{D1} = 0.50$–1.56	333–391		[107]
Spruce bark	Grinding; 180 °C, 12 h	Mix with KOH, 800 °C–1000 °C, 2 h, N_2	Graphene nanosheet arrays	Vertically aligned graphene nanosheets	87.24%–94.68% C, 5.21%–12.63% O	Peaks at 26.0º and 43.3º	**Raman**: D, G, 2D peaks	2028–2385	7.8%–10.3%	[108]
Bamboo timber waste	25% HNO_3, 6 h; + $KClO_3$, 60 °C, 24 h	60% H_2SO_4, 70 °C; 8 h 180 °C	GQDs		41.1% C, 56.9% O	Peaks at 19.0º, 22.62º, 31.9º and 33.9º	Emission at 245, 365 nm, $I_D/I_G = 0.78$			[110]
Coconut shell	Mix with $FeCl_3$, $ZnCl_2$, drying	900 °C, 1 h, N_2	Porous graphene-like nanosheets	Few and multilayer	O/C = 0.05812	Peaks at 26.5º, 44.7º and 65.2º	$I_D/I_G = 0.25$	1874		[109]
Coconut shell	Burning Grinding	400 °C–1000°C, 5 h, air; 10 h ultra-sonication, DI water	rGO				**FTIR**: O–H, CO_2, N–H, C=O, C=C, C–O, C–H peaks. $I_D/I_G = 1.1$–1.7			[111]

(Continued.)

Table 2. (Continued.)

Precursor	Pre-treatment	Treatment/exfoliation	Product	Microscopy	Elemental analysis	Diffraction	Spectroscopy	BET ($m^2\ g^{-1}$)	Yield	References
Coconut shell	Burning Grinding	400 °C–1000°C, 5 h, air; 10 h ultra-sonication, DI water	rGO			Peaks at 24º, 43º	**FTIR**: O–H, C=O, C=C, C–H, C–O			[112]
Coconut coir, shell	Grinding, mix with ferrocene	300 °C, 15 min, air	rGO	Few layers		Peaks at 23.3º, 24.4º	**FTIR**: C=O, C–O, C–OH, O–H. **Raman**: D, G bands, Abs peak at 260 nm			[113]
Coconut fibre	Washing, drying; KOH, 2 h	300 °C 1 h, 750 °C, 3 h, Ar; HCl, 12 h; HNO_3, 12 h S/N doping: mix with S/urea, 450 °C, 40 min, Ar; 750 °C, 30 min, H_2	Porous, S/N-doped GO	0.91–4.19 nm thick,	67%–85% C, 3.9% N, 0.9% S,	Peaks at 24.4, 42.3°	**Raman**: $I_D/I_G = 0.98$–1.18, **FTIR**: C–O, C–O–C, C=C, C–S, C–N	1083–1114		[114]

Table 3. Starting materials, preparation steps and characterization of GRMs produced from plant-derived waste.

Precursor	Pre-treatment	Treatment/exfoliation	Product	Microscopy	Elemental analysis	Diffraction	Spectroscopy	BET ($m^2\ g^{-1}$)	Yield	References
Palm kernel shell, palm leaves, empty fruit bunch	400 °C–900 °C, 3 h, N_2	Improved Hummers'	GO	Porous, layered structure		Peaks at 10.3º, 25º	I_D/I_G = 1.06–1.20 **FTIR**: O–H, C=O, H_2O, C–H, C–O	15–117	26%–37%	[115]
Palm kernel shell	Urea, $FeCl_3$, $ZnCl_2$, 80 °C, 2 h	350 °C, 1 h, N_2; 900 °C, 90 min, N_2	Nanosheets	Few-layers		Peaks at 26.5º, 33.8º, 36.58º	I_D/I_G = 0.32 **FTIR:** N–H, C–N, C=C	351.26	16%	[116]
Flower petals	Drying	800 °C–1600 °C, 30 min, Ar	Graphene	Thin layers	C/O = 82–142		I_D/I_G = 0.37–1.31			[117]
Camellia shells	KOH, 180 °C, 12 h	800 °C, 2 h, Ar	Graphene-like	Ultrathin carbon layers	0.64%–0.73% N	Peaks at 24º, 43º	I_D/I_G= 0.3–1.22	633–1020		[118]
Almond shells	Crushing Drying,	KOH, 700 °C–900 °C, 2 h, N_2	Graphene-like activated carbon	Sheet-like morphology (4–6 layers)		Peaks at 23, 43°	I_D/I_G = 0.83–0.88	1608–2539		[119]
Sugarcane bagasse	Melamine, 180 °C, 10 h	850 °C, 3 h, Ar	N-doped sheets	4–8 layers	0%–14% N	Broad peaks at 26º, 44º	I_D/I_G = 1.02–1.15			[120]
Sugarcane bagasse	Drying in the sun, grinding	Ferrocene, 300 °C, 10 min, air	GO	Single layer sheets			**FTIR**: O–H, C=O, C–O–C, C–OH			[121]
Sugarcane bagasse	Drying in the sun, grinding	60 °C, 4 h; sonication in toluene	CQDs	1–18 nm QDs			**FTIR**: O–H, C=O, COOH, C–O, C–H, CO_2 Abs peak at 270–350 nm.			[121]
Sugarcane bagasse, orange peel, rice bran	Washing, drying, grinding	Ferrocene, 300 °C, 15 min	GO	Few-layers, 1–9 nm thick		Main peak at ∼13º	**FTIR**: N–H/C–H/O–H, H2O, C=C, $–NH_2$, CO–O–CO, $-CH_2$			[122]
Pomelo peel	Freeze drying, mixing with HAc, H_2O_2; 120º C, 3 h	800 °C, 3 h, Ar	Graphene-like porous carbon nanosheets	Porous, 10–100 nm thick nanosheets		Broad peak at 20º–26º, weak peak at 44.3º	I_D/I_G = 1.04	Up to 808.9		[123]
Wheat straw	3 M KOH, 150 °C, 6 h	800 °C for 3 h, N_2; 2600 °C, 5 min, Ar	Few-layer	1.2-3-5 nm thick	98.88% C, 1.12% O	Peaks at 26.5º, 42.4°, 44.3°, 54.6º	I_D/I_G = 0.73	35.5	11.3%	[124]

(Continued.)

Table 3. (Continued.)

Precursor	Pre-treatment	Treatment/exfoliation	Product	Microscopy	Elemental analysis	Diffraction	Spectroscopy	BET ($m^2\ g^{-1}$)	Yield	References
Straw	80 °C, 48 h, air; 450 °C, 45 min, N_2	Modified Hummers'	GO	Nanosheet 60–100 nm lateral size		Peaks at 26.60°, 43.09°	**FTIR**: C=C, C=O, O–H, C–N, C–H			[125]
Peanut shells	H_2SO_4, 180 °C, 48 h	KOH, 800 °C, 1 h, Ar	Nanosheet	Sponge structure comprised of nanosheets	85.91%–89.45% C, 9.7%–13.51% O, 0.58%–0.96% N	Broad peaks at 26°, 44°	$I_D/I_G = 0.41$–0.62	1998–2396	19%–29%	[126]
Peanut shells	—	1200 °C, 6 h, Ar		Sponge structure made of nanosheets	92.94%–93.70% C, 5.57%–6.09% O, 0.73%–0.97% N	Broad peaks at 26°, 44°	$I_D/I_G = 1.01$–1.10	78–476	35%	[126]
Soybean okara	Drying	800 °C, 2 h, N_2	N-doped nanosheets		88.40% C, 9.43% O, 2.17% N	Broad peaks at 24°, 43°	$I_D/I_G = 1.092$ **FTIR**: C–N, C=O, CH_2	133		[127]
Soy flour	Mix with glucose	180 °C, 8 h	N-doped C spheroids	Few-μm graphitic spheroids	74.10% C, 2.22% N, 23.68% O	Broad peaks at 21°, 26°	Abs peak at 250 nm, **FTIR**: O–H, C–H, C=C, C=N, C–N, C–O, =C–H	7.43		[128]
Dead neem leaves	1000 °C, 5 h, Ar; grinding	H_2SO_4, HNO_3, 90 °C, 5 h	GQDs	5–6 nm lateral size. 0.4–1.7 nm (1–5 layers)	C/O = 3.17	Peak at 24–25°	Abs peak at ∼300 nm **FTIR**: O–H, N–H, -NH_2, C–N, C–O			[129]
Dead camphor leaves	1200 °C, 4 min, N_2	15 min sonication in $CHCl_3$ with D-Tyrosine	Few-layer graphene	∼7 layers		Peaks at 25.5°, 26.2°	$I_D/I_G = 0.99$	296	0.8%	[130]
Rice husk	Burning in air	KOH, 850 °C, 2 h, air	Graphene	Nano-sized crystalline graphene	91.6% C, 6.6% O, 2% Si, 0.2% Ca	Broad peaks at ∼24°, 43°	$I_D/I_G = 0.85$–1.34		10%	[131]
Hemp	H_2SO_4, 180 °C, 24 h	KOH, 700 °C–800 °C, 1 h, Ar	Nanosheets	10–100 nm thick	93.39–94.33% C, 4.19%–5.60% O, 0.9%–1.48% N	Broad peaks at ∼24°, 44°	$I_D/I_G = 0.85$–0.93	1505–2287		[132]

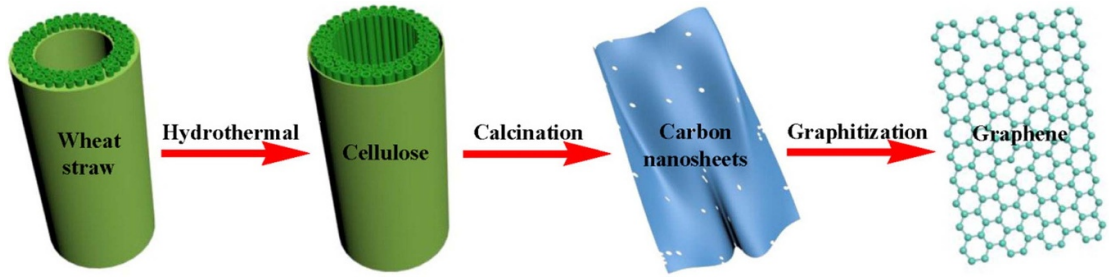

Figure 4. Thermal transformation of wheat straw into graphene. Reprinted from [124], Copyright © 2016 Elsevier B.V. All rights reserved.

in table 3. Using a similar procedure, almond shells have been reported as the starting material to prepare graphene-like activated carbon [119]. The shells were crushed and dried, followed by a reaction with KOH at 700 °C–900 °C for 2 h in N_2 atmosphere. As a result, an activated carbon with few-layers (4–6), nanosheet-like morphology and high surface area (up to 2539 m^2g^{-1}) was obtained. XPS analysis revealed the presence of C and O, but no quantitative and detailed composition is given. In the work of Babu *et al*, biowaste bagasse was treated with melamine at 180 °C, followed by 3 h at 850 °C in Ar atmosphere [120]. Nitrogen doped, graphene-like carbon sheets were obtained, made of 4–8 layers and containing up to 14 at.% nitrogen. In 2019, Baweja and co-workers reported the use of two different methods for the conversion of sugarcane bagasse into GO and CQDs [121]. In both cases, the starting material was dried in natural atmosphere under the sunlight and ground to fine powder. In order to produce GO, the material was treated with ferrocene at 300 °C in air, resulting in oxidised single and few-layer nanosheets. To obtain CQDs, the dried and ground bagasse was treated at 60 °C, followed by a sonication step in toluene. As a result, QDs of 1–18 nm in size were obtained, with emission peaks at 409–437 nm. Recently, Hashmi *et al* reported the formation of GO NPs from sugarcane bagasse, orange peel and rice bran [122]. These waste materials were treated with ferrocene at 300 °C and the resulting material consisted on thin, layered sheets, 1–9 nm thick, with both nitrogen and oxygen functional groups, as evidenced by FTIR characterization. Pomelo peels have also recently been reported as the starting material for the preparation of graphene-like porous carbon nanosheets [123]. To this end, the peels were treated first with acetic acid and hydrogen peroxide at 120 °C, and then heated to 800 °C for 3 h in an Ar atmosphere. SEM and TEM analysis showed the material was comprised of porous, 10–100 nm thick nanosheets, with a BET surface area of 808.9 m^2g^{-1}. XPS and EDX analysis show only C and O signals, but no quantitative composition is reported.

Straw waste has also been proven to be a viable option for its conversion into graphene and GO, as evidenced by the works of Chen *et al* [124] and Goswami *et al* [125]. In the first work, the authors firstly treated wheat straw with KOH at 150 °C, following by thermal treatments at 800 °C in N_2 atmosphere and 2600 °C in Ar atmosphere (figure 4). As a result of these high temperature treatments, the polymers present in the straw (i.e. cellulose, hemicellulose and lignin) were transformed into a layered structure, resulting in few-layer nanosheets as evidenced by SEM, TEM and AFM imaging, with low amounts of oxygen (∼1 at.% O). Following a different approach, Goswami and co-workers treated straw by means of two thermal steps, one in air at 80 °C and one in N_2 atmosphere at 450 °C. The resulting product was then used in a modified Hummers' method, yielding GO nanoplatelets with lateral sizes between 60 and 100 nm. Using the procedure shown in figure 5, in 2015 Ding *et al* used peanut shells for the preparation of two different carbon materials, designated as nanosheet carbon and ordered carbon [126]. For the nanosheet preparation, peanut shells were first treated with H_2SO_4 at 180 °C, and then with KOH at 800 °C in Ar atmosphere. This process transformed the starting materials into a sponge-like structure comprised of nanosheets that displayed very high surface area (1998–2396 m^2g^{-1}) and variable oxygen and nitrogen content (9.7–13.51 at.% O, 0.58–0.96 at.% N). For the ordered carbon preparation, a one-step procedure consisting on the carbonization of the starting materials at 1600 °C in Ar atmosphere, which yielded a material with similar structure than the previous one but with lower surface area (78–476 m^2g^{-1}) and heteroatom contents (5.57–6.09 at.% O, 0.73–0.97 at.% N). Following a thermal procedure, Sha and co-workers reported the processing of soybean okara into nitrogen-doped mesoporous graphene-like nanosheets [127]. The dried okara was carbonized at 800 °C in N_2 atmosphere and a layered, oxidised material was obtained (9.43 at.% O, 2.17 at.% N). Soybean flour has been also used as starting material, by treating a mixture with glucose

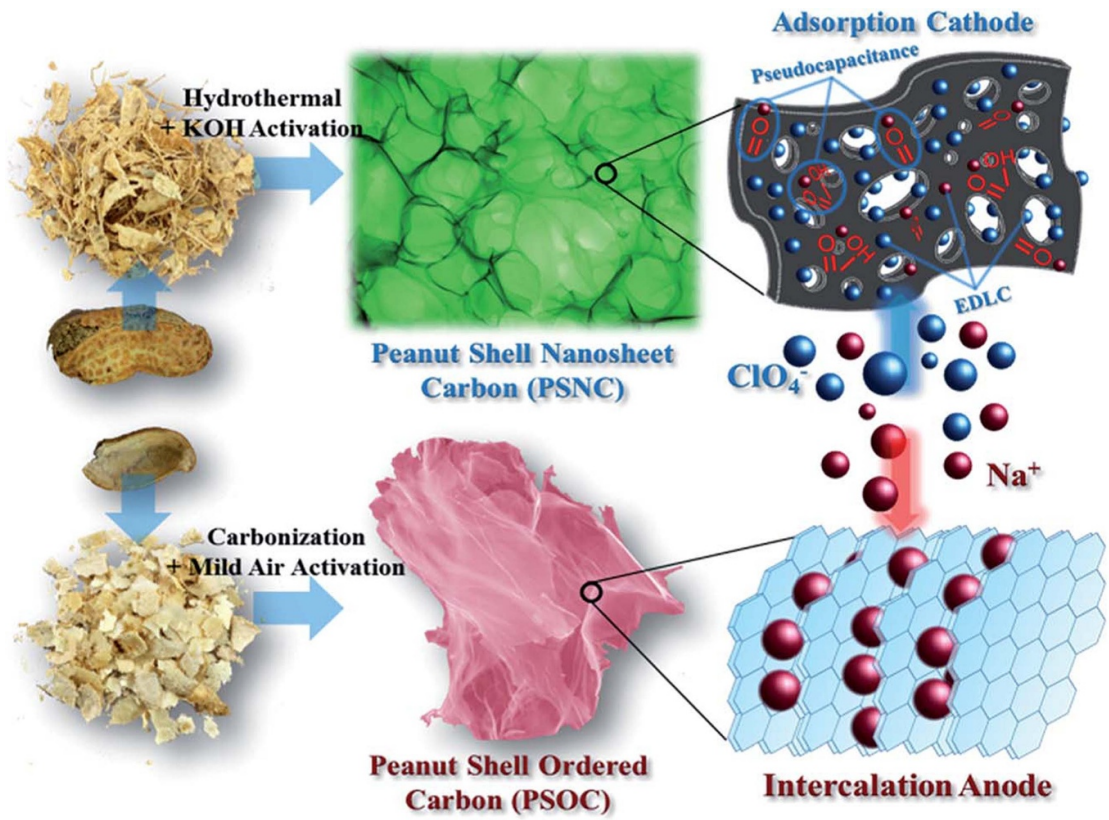

Figure 5. Nanosheet carbon and ordered carbon prepared by thermal treatment of peanut shells. Reproduced from [126] with permission of The Royal Society of Chemistry.

at 180 °C for 8 h in an autoclave [128]. The resulting product was characterized as few-μm carbon spheroids composed of graphitic layers that displayed the typical graphite/graphene XRD peaks. FTIR analysis revealed the presence of N and O functional groups, and XPS showed a composition of 74.10 at.% C, 2.22 at.% N, 23.68 at.% O. Dead leaves have also been reported as a source for the preparation of GQDs (neem leaves in Suryawanshi *et al* [129]) and few-layer graphene (camphor leaves in Shams *et al* [130]). Neem leaves were pyrolyzed at 1000 °C in Ar atmosphere to yield turbostratic carbon, which was subsequently treated with H_2SO_4 and HNO_3 at 90 °C, yielding GQDs 0.4–1.7 nm thick (1–5 layers), 5–6 nm in lateral size and with a C/O ratio of 3.17. Shams and co-workers used camphor leaves that were pyrolyzed at 1200 °C in N_2 atmosphere, and then sonicated in chloroform with the aid of D-tyrosine. The dispersed product was made of thin nanosheets (2.37 nm, ~7 layers) and the process showed a low yield of 0.8%. In 2014, Muramatsu *et al* used rice husk for the preparation of graphene in a two-step thermal procedure in air[131]. The starting material was first burned and then treated with KOH at 850 °C, yielding nano-sized crystalline graphene with residual amounts of oxygen, silicon and calcium (6.6 at.% O, 2 at.% Si, 0.2 at.% Ca). Carbon nanosheets were obtained from hemp waste from Wang and co-workers, using a preparation method consisting in the treatment with H_2SO_4 at 180 °C followed by a chemical activation step with KOH at 700 °C–800 °C in Ar atmosphere [132]. The resulting material displayed an interconnected, sheet-like structure with sheets 10–100 nm thick, with high surface area (1505–2287 m^2g^{-1}) and residual amounts of oxygen and nitrogen (4.19–5.60 at.% O, 0.9–1.48 at.% N).

2.1.4. Food waste

Food waste has also successfully been processed through (combined or separated) thermal and chemical treatments to produce GRMs by a number of research groups. Panahi-Kalamuei *et al* have reported the use of waste bread for the preparation of graphene and GQDs by means of a low temperature, two-step procedure [133]. The bread waste was first heated in deionized water at 70 °C–80 °C to produce a gel suspension, and then to 180 °C in an autoclave. As a result, a mixture of GQDs, few- and multilayer graphene was obtained, which displayed peaks in XRD diffractograms corresponding to a layered structure. Coffee waste has been reported as a starting material to be processed into graphene and GO, in the works of Wang *et al* [134] and Sundriyal *et al* [135] respectively. In the first work, the authors used a microwave plasma treatment to transform the starting material into fibres made of slightly oxidised, few-layer graphene sheets with yield between 10% and 20%. In the second work, ground coffee was mixed

with $ZnCl_2$ and then pyrolyzed at 900 °C in a N_2 atmosphere, with a final oxidation step with H_2O_2 at 65 °C. Porous, layered GO sheets were obtained as a result, displaying oxygen functional groups, as evidenced by FTIR, as well as a high surface area of 1033.65 m^2g^{-1}. Tea waste has also been used for the preparation of GO by means of a carbonization step at 650 °C in Ar atmosphere, followed by a modified Hummers' method [136]. In this work, Amir Faiz and co-workers obtained multilayer GO sheets but no quantification on Oxygen content or number of layers was provided in the paper. Using the same waste material, Abbas *et al* prepared GQDs in a multi-step process [137]. First, the tea leaves were washed, dried, crushed and heated to 500 °C. In a following step, the resulted materials were mixed with HNO_3, subjected to microwave heating and finally heated to 200 °C for 8 h. The end product consisted of GQDs with size of 0.5–3.5 nm and with a composition of 56.45 at.% C, 36.73 at.% O, 4.76 at.% N, and they also show fluorescence emission at ∼430 nm. Following a low temperature approach, potassium-doped GO nanosheets were prepared by Tewari *et al* using oak fruits as the carbon source [138]. To this end, the starting materials were washed, ground and heated to 120 °C, yielding a brown solid that was dispersed in distilled water. Analysis of the final product revealed the presence of photoluminescent GO nanosheets comprised of ∼4 layers, and its doping was evidenced by EDX (6.81 at.% K).

Tables 3 and 4 show that the last two methodologies tend to give different forms of GRMs; in particular, in the case of food waste, it seems to be quite difficult to achieve any carbon form similar to that of pristine graphene.

2.1.5. Monosaccharides hexoses

Simple molecules, such as glucose and sucrose, have been two of the earliest and most commonly reported precursors for the preparation of GRMs. The first example of the use of glucose can be found in the work of Li *et al* in 2012 [139]. In order to obtain graphene nanosheets, glucose was treated with dicyanamide at 600 °C to form g-C_3N_4, which was then decomposed at 800 °C, both steps being carried out in N_2 atmosphere. The resulting nanosheets were mono- and multilayers, with a relatively high surface area of 820 m^2g^{-1} and a chemical composition of ∼93 at.% C, with the remaining being oxygen and nitrogen. In 2013, Wang and co-workers reported the production of 3D structures, named 'strutted graphene', by means of a polymer intermediate formation (figure 6) [140]. Glucose was polymerized in the presence of NH_4Cl at 250 °C, and the salt decomposition gave rise to bubbles that promoted the 3D strutted structure. In a second step, the polymer-containing solid was graphitized at 1350 °C in Ar atmosphere to yield GRMs. SEM and AFM analysis confirmed the formation of nanosheets that were found to be ∼2.2 nm thick (six layers) and ∼100 μm lateral size, with 99% of sp^2 carbon and high surface area and conductivity (1005 m^2g^{-1} and 20 000 S m^{-1} respectively). The Raman spectrum showed sharps D, G and 2D peaks, indicating the presence of low amount of defects; being a defective GRM, Raman spectroscopy cannot be used to determine the thickness from the 2D peak shape [71]. Few-layer graphene has also been produced from glucose by Zhang *et al*, in a thermal process where $FeCl_3$ acts as both the template and catalyst [141]. Glucose and $FeCl_3$ were mixed in water and dried at 80 °C in air, and subsequently calcined at 800 °C–1000 °C in Ar atmosphere. In the second step, Fe-catalysed graphitization of the glucose occurred, yielding a solid product comprised of few-layers graphene with a composition of 98.5 at.% C and 1.5 at.% H and various amounts of defects (I_D/I_G = 0.1–1.1). CQDs have been prepared from glucose by Xie *et al* by means of a hydrothermal process [142]. Glucose was heated at 200 °C in an autoclave, and as a result CQDs with layered structure surrounded by amorphous carbon were obtained. CQDs showed small and narrow size distribution (∼5.15 ± 0.83 nm), and a chemical composition consisting of carbon and oxygen (60.2 at.% C–C/C=C, 21 at.% C–O, 9.1 at.% C=O, 9.7 at.% COOH). Also using glucose, Yao *et al* prepared GQDs by subjecting a mixture with ethylene glycol to microwave heating for 9 min [143]. The resulting GQDs were ∼1.7 nm thick and 2.6-3.8 nm in lateral size, showed fluorescence emission at 440–492 nm and had a composition of 63.4 at.% C and 36.6 at.% O. In 2013, Pan *et al* produced nitrogen-doped graphene from sugar and urea by means of a high-temperature treatment [144]. The mixture of reagents was pyrolyzed at 800 °C–1000 °C in Ar atmosphere, resulting in wrinkled, interconnected graphene nanosheets ∼2 nm thick (5–7 layers). The material showed a polycrystalline nanostructure, and XPS analysis showed that the surface chemistry was predominantly made of carbon, with varied amounts of oxygen and nitrogen, related to the starting materials and temperature difference treatments (2.61–2.96 at.% O, 3.02–11.2 at.% N). Parvathi *et al* prepared graphene-sand composites by treating mixtures of sugar and sand in a two-step process [145]. The mixtures were first heated at 200 °C and then at 750 °C, in both cases in a reducing atmosphere. The resulting material was made of graphene sheets anchored to the sand surface, as evidenced by the SEM images. EDAX analysis showed the graphene was composed of 43.20 at.% C, 36.97 at.% O, 10.75 at.% S, 5.99 at.% Si, with traces of aluminium, calcium and iron. In 2017, few-layer graphene was prepared from sugar by Yassin and co-workers [146]. Sugar was ground with ammonium acetate and sintered at 1100 °C in Ar atmosphere, resulting in the graphitization and conversion of sugar into 4–7 layers' graphene nanosheets. This material displayed a high surface area varying from 477.42–1098.99 m^2g^{-1} and

Table 4. Starting materials, preparation steps and characterization of GRMs produced from food waste.

Precursor	Pre-treatment	Treatment/exfoliation	Product	Microscopy	Elemental analysis	Diffraction	Spectroscopy	BET ($m^2\ g^{-1}$)	Yield	References
Waste bread	DI water, 70 °C–80 °C	180 °C, 12 h	Graphene, GQDs	Mix of graphite, quantum dots and few/multi-layer graphene		Peaks at 10º, 20º				[133]
Coffee	Drying	Microwave Plasma treatment (2.45 GHz, 900 W)	Graphene-sheet fibers	Few-layer sheets.			$I_D/I_G = 1.1$		10%–20%	[134]
Coffee	Drying; $ZnCl_2$, 4 d	900 °C, 1 h, N_2; H2O2, 65 °C, 4 d	Porous GO	Layered graphene-like sheets		Peaks at 22.6º, 42.6º	$I_D/I_G = 0.98$ **FTIR**: N–H, C–H, O–H, C=O, C=C, NO_3^-, C–C, C–H, $–SO_3H$ p	1033.65		[135]
Tea waste	650 °C, 3 h, Ar	Modified Hummers'	GO	Multiple layer of carbon sheet		Peak at 23.16º	$I_D/I_G = 0.84–0.96$ **FTIR**: C–O, C=C, C–O, O–H peaks			[136]
Tea waste	Washing, drying, grinding; 500 °C, 3 h	HNO_3, 100–900 W microwave, 15–180 min; 200 °C, 8 h	GQDs	∼0.5-3-5 nm QDs	56.45% C, 36.73% O, 4.76% N		$I_D/I_G = 0.98$ **FTIR**: O–H, N–H, C=O, C=C, C–C/C–H, C–N, C–O Emission peak at ∼430 nm, Abs peak at ∼270–280 nm		Up to 84.5%	[137]
Oak fruits	Washing, crushing	120 °C, 4 h, air	K-doped GO	∼4 layers	6.81% K	Peaks at 13.6º, 27.1º, 39.0º	**FTIR**: O–H, C=O, C–C, C-O–C, C–O Abs peak at 270 nm. Emission peak at 461 nm.			[138]

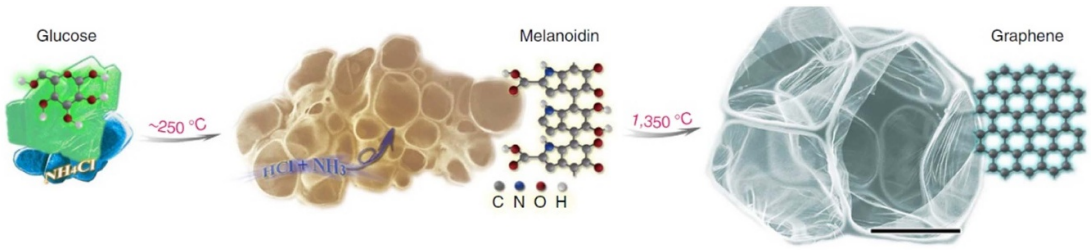

Figure 6. 3D strutted graphene prepared from glucose and ammonium chloride. Reprinted by permission from Springer Nature Customer Service Centre GmbH: Springer Nature, Nature Communications [140], Copyright © 2013, The Author(s).

the characteristic D and G Raman bands of graphene materials, but no information on the chemical composition was given.

2.1.6. Animal-derived waste

A few animal-derived wastes (i.e. silk, chitosan, gelatine, chicken feathers, chitin) have been successfully used as carbon sources for the preparation of graphene materials. Hierarchical porous nitrogen-doped carbon nanosheets were prepared by Hou *et al* by means of a high temperature of silk [147]. The starting material was first mixed with $ZnCl_2$ and $FeCl_3$ and heated at low temperatures (60 °C and 80 °C) to form a carbon precursor that was then annealed at 900 °C in a nitrogen atmosphere. In this process, the metallic salts first facilitate the dissolution of silk, and then act as activation-graphitization agents, promoting the transformation of the starting material into graphene-like nanosheets. The resulting product is made by a stacking of thin nanosheets (~2 nm, 4–5 layers) with a high surface area of 2494 m^2g^{-1} and a chemical composition of 90.3 at.% C, 4.1 at.% N and 4.1 at.% O. The group of Prof. García reported in 2012 a two-step thermal treatment of chitosan that yielded N-doped graphene nanosheets [148]. To this end, chitosan was first annealed at 200 °C and then pyrolyzed at 800 °C, both steps being carried out in Ar atmosphere. The first step resulted in the conformational relaxation of the polymer, which the authors mention is beneficial for the quality of the graphene material obtained after the second step. As a result of this process, single and few-layer graphene nanosheets with single crystalline domains were produced, and XPS analysis revealed ~10.71 at.% of N content. In 2014, the same group described another process to obtain N-doped graphene, also using chitosan as the starting material [149]. This process involved the formation of chitosan aerogels through precipitation with NaOH, and then treating them in a two-step process similar to the one previously reported, first at 200 °C–280 °C and then at 200 °C–900 °C. As a result, 1–5 nm thick graphene nanosheets were obtained, with nitrogen contents that varied between 5.4 and 16.2 at.% with the pyrolysis temperature. In 2018, Zhang *et al* prepared CQDs from chitosan in a one-step hydrothermal procedure [150]. Chitosan was heated at 200 °C in ethanol, and ~4 nm, amorphous CQDs were obtained as a result of this process. The material displayed oxygen and nitrogen functional groups, as evidenced by XPS and FTIR analysis, but no quantification was provided. Its PL emission was measured and the CQDs showed emission peaks at 400–550 nm as a function of the excitation wavelength. Very recently, Gao *et al* used a two-step process to transform chitin into 2D porous carbon nanosheets [151]. Chitin naturally displays a layered structure and, in order to weaken the interlayer interactions, it was first treated with phytic acid and hydrogen peroxide via a hydrothermal process, yielding ~10 nm thick, porous chitin nanosheets. This material was then carbonized at 700 °C–900 °C under Ar atmosphere to obtain 2D porous carbon nanosheets ~3.6 nm thick, with an elemental composition of 85.49 at.% C, 4.53 at.% N, 7.89 at.% O, 1.35 at.% P, $I_D/I_G = 0.82–0.87$ and a surface area of 717–1049 m^2g^{-1}. Gelatine was used by Ling *et al* to obtain B,N-doped carbon nanosheets, by means of a thermal treatment in the presence of boric acid [152]. The reagents were annealed at 900 °C in N_2 atmosphere: during this process the gelatine is transformed into carbon nanosheets via a thermal-induced polycondensation and carbonization, while boric acid decomposes into boron oxide. The resulting material was made of 5–8 nm thick nanosheets with lateral sizes in the 100–200 nm range, and having a C/O ratio of 7.72 and 8.6 at.% N, 3.3 at.% B. In 2017, Li and coworkers used chicken feathers in a three-steps thermal procedure to prepare a multi-layered graphene-phase biochar [153]. The starting material was first treated at 220 °C to crosslink and reformulate its structure, and then carbonized at 450 °C. The carbonized product was subsequently mixed with KOH and heated at 800 °C, with all the steps being carried out in Ar atmosphere. The product of this process was multilayer graphene, as evidenced by SEM and TEM imaging, and its composition was elucidated by means of elemental analysis, resulting in 66.06–84.77 at.% C, 9.85–16.41 at.% O, 4.28–14.15 at.% N. The material exhibited the characteristic D, G and 2D bands in the Raman spectrum, as well as oxygen and nitrogen containing functional groups signals in FTIR and a very high surface area of 1838.86 m^2g^{-1}. More recently,

Pajarito *et al* reported another approach for the use of chicken feathers as a starting material for the preparation of graphite nanoplatelets [154]. Chicken feathers were first washed and dried, carbonized at 400 °C for 5 h, and treated with $FeCl_3$ at 60 °C. The resulting material was subsequently sonicated in an IPA aqueous solution, yielding GNPs with thicknesses in the tens of nm range, and lateral sizes below 1 μm. GNPs obtained with this method displayed C=C, C=O and –CONH signals, as well as typical XRD and Raman signals for graphitic materials.

Amongst the methods discussed so far, monosaccharides hexoses and animal-waste based precursors gives in most cases GRMs with nanosheet morphology and lowest oxygen content, although impurities or other defects may be included in relatively low amount (tables 5 and 6).

2.2. Non-biological sources

A few products from non-biological sources have been recently used as starting materials for the preparation of GRMs. Namely, the use of discarded batteries, graphite, coal, fuel oil and polymers derived from plastic. Owing to the chemical composition, morphology and structure of each waste material, different approaches have been taken. Graphite materials can be processed with common exfoliation procedures, however non-graphitic carbon sources such as coal, fuel oil and polymers require high-temperature graphitization steps, preferably in inert or reducing controlled atmosphere, as seen for materials from biological sources.

2.2.1. Discarded batteries

Non-rechargeable batteries are not as extensively used because of the widespread adoption of built-in rechargeable batteries; however, they still constitute a considerable source of waste today, as well as an environmental concern due to their high environmental risk if incorrectly disposed [155]. Among the variety of commonly used batteries, some categories require the use of graphite in their electrodes. Namely, Zn–C dry cells use graphite rods as the cathode electrode, and the more common Li-ion batteries (LIB) make use of a paste containing graphite powder in the anode electrode. Both of these graphitic materials can be easily recovered from discarded batteries and processed for their use in the preparation of GRMs, as several research groups have demonstrated in recent years. This approach has an inherent advantage when compared with other carbon sources discussed later in this review, as the starting materials already have a graphitic structure and can be readily exfoliated without the need of a graphitization process.

The first example of graphene materials prepared from waste batteries, to the best of our knowledge, is given by the work of Roy *et al* in 2016 [156]. The authors recovered graphite rods from discarded Zn–C batteries, washed and ground them, and used the resulting powder as a substitute for commercial graphite for the preparation of GO through Hummers' method. GO nanosheets were obtained with a composition of 45.72 at.% C, 49.21 at.% O. A significant contamination of 1.56 at.% Al and 3.51 at.% Si, derived from the electrochemical processes during battery life. This GO could be reduced by reaction with hydrazine, yielding rGO with a composition of 74.54 at.% C, 24.72 at.% O and a small amount of contaminants (0.48 at.% Al, 0.26 at.% Si). A similar route was described by Rahmawati *et al*, using the same waste materials [157]. GO was obtained by a modified Hummers' method, although a wide range of metal oxide impurities (i.e. MnO, Na_2O, SO_3, K_2O, SiO_2, MgO, CaO, Al_2O_3) were found. Graphene production by ECE [38, 158] has also been demonstrated starting from graphite rods derived from Zn–C batteries, owing to the ease of use of the rods as electrodes. Bandi *et al* performed anodic ECE using 0.5 M H_2SO_4, applying 10 V for a duration of 2 h [159]. As represented in figure 7(a), the rods were exfoliated into multilayer GO nanosheets with an oxygen content of 22.8 at.%. The material obtained was then thermally reduced at 650 °C to yield rGO with 13.6 at.% oxygen. Another example of graphene produced by ECE from discarded battery graphite rods is found in the work of Prakoso and co-workers [160]. In this work, the authors reported anodic ECE using solutions of poly(sodium 4-styrenesulfonate) (PSS) as the electrolyte, and applied potentials of 5–8 V for 4 hs to exfoliate the rods into graphene. The exfoliated material is given by few- to multilayer nanosheets, and the functionalization with PSS molecules allows its water-dispersibility. Due to the anodic ECE conditions the material becomes significantly oxidised, as evidenced by XPS and FTIR. However, the precise oxygen content was not reported.

Some examples of the use of graphite from discharged LIBs have been reported recently. Using a modified Hummers' method, Wang *et al* obtained few- and multilayer GO nanosheets with an oxygen content of 26.3 at.%. The material could then be thermally reduced into rGO (17.2 at.% O), and showed small amounts of Si contamination (∼0.4 at.%) [161]. A similar route was reported by Li *et al*, who treated the electrode graphite powder with H_2SO_4, $KMnO_4$ and peroxyacetic acid to obtain rGO nanosheets [162]. The final material was comprised of few- and multi-layer nanosheets and displayed a higher oxidation degree than the one obtained from commercial graphite in the same process (C/O ratios of 1.79 and 4.25, respectively). Using graphite recovered from different types of LIBs in a modified Hummers' method, Yu *et al* recently prepared GO nanosheets [163]. The final product was made of ultrathin nanosheets and had oxygen content of 33–36 at.%, depending on the starting material and showed no impurities from the other battery

Table 5. Starting materials, preparation steps and characterization of GRMs produced from monosaccharides hexoses.

Precursor	Pre-treatment	Treatment	Product	Microscopy	Elemental analysis	Diffraction	Spectroscopy	BET ($m^2\ g^{-1}$)	Yield	References
Glucose	Dicyanamide, 600 °C, 4 h, N_2	800 °C, 1 h, N_2	Graphene	Monolayer and multilayer sheets.	∼93% C, rest is O and N	Peak at ∼26º	**Raman**: D, G bands.	820	28%–60%	[139]
Glucose, sucrose	NH_4Cl, 250 °C	1350 °C, 3 h, Ar	Graphene	Nanosheets, 2.2 nm thick (6 layers), ∼100 μm lateral size		Peak at 26º	**Raman**: D, G, 2D bands	1005	16%	[140]
Glucose	$FeCl_3$, drying at 80 °C, 24 h, air	700 °C, 6 h, Ar	Graphene	Few-layer graphene sheets	98.5% C, 1.5% H	Peak at 26º	**Raman**: $I_D/I_G = 0.35$		40%	[141]
Glucose	—	Water, 200 °C, 6 h	CDs	Layered structure surrounded by amorphous carbon, ∼5.15 nm	60.2% C–C/C=C, 21% C–O, 9.1% C=O, 9.7% COOH	Broad peak at ∼22.5º	**Raman:** D, G bands. **FTIR**: O–H, C=O, O–C–H, C–O–H, C–O, C–C, C–H emisión peaks at ∼500, 650 nm			[142]
Glucose	Mixing with ethylene glycol	800 W microwave, 9 min	GQDs	2.6–3.8 nm in size, ∼1.7 nm thick	63.4% C, 36.6% O	Peak at 24º	**FTIR**: O–H, C–H, C=O, C=C, C–C, C–O, Main Abs peak at 230 nm Emission peak at 440–492 nm			[143]
Sugar and urea mix	Dissolve in water, evaporate	800 °C–1000 °C, 1 h, Ar	N-doped graphene	Interconnected and wrinkled sheets 5–7 layers	86.03%–94.37% C, 2.61%–2.96% O, 3.02%–11.2% N		$I_D/I_G = 1.07–1.28$	461.9–579.4		[144]
Sugar	Mix with sand, 200 °C, 1 h, reducing atmosphere	750 °C, 3 h, reducing atmosphere	Graphene-sand composite	Graphene sheets	43.20% C, 36.97% O, 10.75% S, 5.99% Si. Traces of Al, Ca, Fe.	Peaks at 20. 97º, 26.73º, 42.54º, 45.875º, 54.9, 59º, 64.11º	Broad Abs peak at ∼302 nm. **FTIR**: C=C, C–O, O–H, C–H, =C–H			[145]
Sugar	Ammonium acetate, grinding	1100 °C, 1 h, Ar	Graphene	3–4 layers		Peak at 27.5º	**Raman**: D, G bands.	477.42–1098.99		[146]

Table 6. Starting materials, preparation steps and characterization of GRMs produced from animal waste.

Precursor	Pre-treatment	Treatment/exfoliation	Product	Microscopy	Elemental analysis	Diffraction	Spectroscopy	BET ($m^2\ g^{-1}$)	Yield	References
Silk	$ZnCl_2$, $FeCl_3$, 60 °C, 4 h; 80 °C	900 °C, 1 h, N_2	Porous N-doped carbon nanosheets	4–5 layers	90.3% C, 4.1% N, 4.1% O (wt %)	Peaks at 26°, 44°	$I_G/I_D = 1.15$	2494		[147]
Chitosan	200 °C, 2 h, Ar	800 °C, Ar	N-doped graphene	Single- and few-layers	10.71% N		**Raman**: D, G bands. Abs peak at 250 nm			[148]
Chitosan	4 M NaOH, washing, drying	200 °C–280 °C, 2 h, Ar; 200 °C–900 °C, 2 h, Ar	N-doped graphene	1–5 nm thick	5.4%–16.2% N		**Raman**: D, G bands			[149]
Chitosan	—	Ethanol, 200 °C, 12 h	CQDs	∼4 nm diameter, amorphous particles		Broad peak at ∼21°	Abs peak at 263 nm Emission peaks at 400–550 nm **FTIR**: O–H, C–H, NH_2, N–H, C–NH, C–N=, C–C, C–O			[150]
Chitin	Phytic acid, H_2O_2, 30 min sonication; 110 °C, 8 h	700 °C–900 °C, 2 h, Ar	2D hierachical porous carbon nanosheets	3.6 nm thick and porous sheets	85.49% C, 4.53% N, 7.89% O, 1.35% P N, O, P distributed uniformly	Broad peaks at ∼ 24.5°, 43.2°	$I_D/I_G = 0.82$–0.87	717–1049		[151]
Gelatin	Mix with boric acid	900 °C, 1 h, N_2	B,N-doped carbon nanosheets	5–8 nm thick, 100–200 nm lateral size	C/O = 7.72, 8.6% N, 3.3% B	Broad peat at 26°	$I_D/I_G = 1.27$	416		[152]
Chicken feathers	220 °C, 8 h, Ar; 450 °, 1 h, Ar	KOH, 800 °C, 1 h, Ar	Multilayered graphene-phase biochar	Multilayer graphene	66.06%–84.77% C, 9.85%–16.41% O, 4.28%–14.15% N		**Raman**: D, G, 2D bands. **FTIR**: –OH, -COOH, C–O, C–N, C=O, C–H, N–H	1838.86		[153]
Chicken feathers	400 °C, 5 h; $FeCl_3$, 60 °C, 5 h	Sonication in 40% IPA aq solution	Graphite nanoplatelets	Tens of nm thick, <1 μm lateral size		Broad peak at ∼25°	$I_D/I_G = 0.56$ **FTIR:** C=C, C=O, -CONH		4.8%	[154]

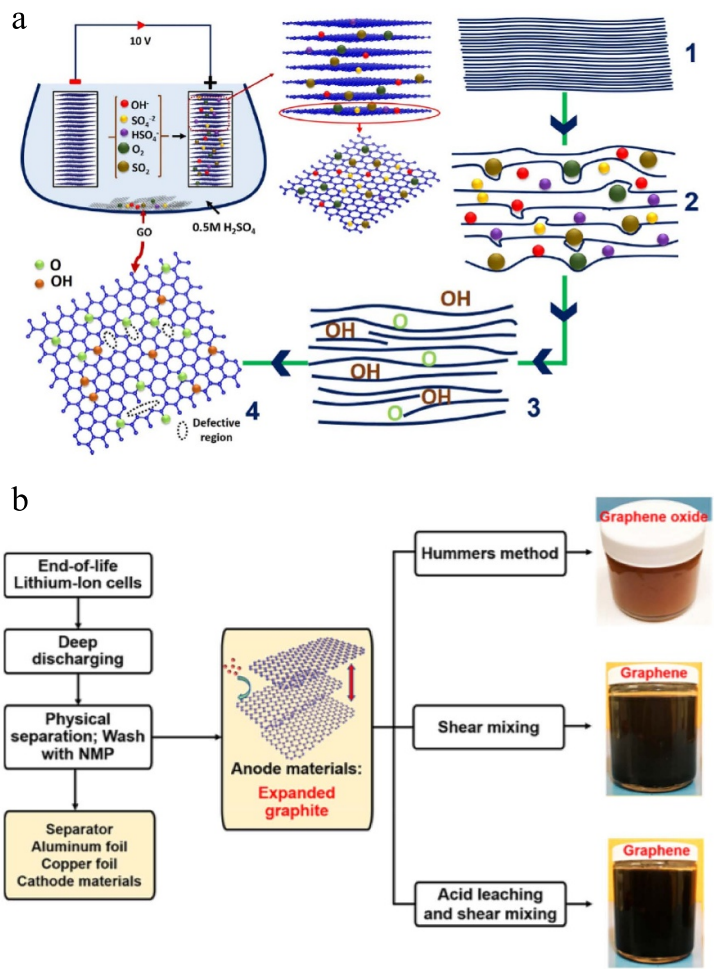

Figure 7. Graphene and GO preparation from waste batteries. (a) ECE of Zn–C battery anodes. (b) Hummers' oxidation, shear mixing of Li-ion cathode graphite. Reprinted from [159], © 2018 Elsevier B.V. All rights reserved. Reprinted with permission from [164]. Copyright © 2019, American Chemical Society.

components. In 2019, Zhang and co-workers reported the use of discharged LIB anodes by exploiting several routes, as depicted on figure 7(b) [164]. The authors described the preparation of GO using Hummers' method, and the resulting material was mostly made of monolayers with an oxygen content of 40.4 at.%. In the same work, the authors used the discharged anodes to prepare graphene nanosheets by means of shear mixing [26, 38, 53]. Their graphene dispersions were comprised of few-layer nanosheets (<7 layers) and displayed a higher colloidal stability than those prepared by the same method with commercial graphite, showing some degree of water dispersibility after several days. This behaviour was attributed to the functional groups in the material, as evidenced by the XPS spectra of the dispersed nanosheets (11.2 at.% O and up to 3.5 at.% F, from the anode binder). In further experiments, H_2SO_4 treatment of the discharged anodes prior to shear mixing increased the exfoliation yield up to 87%, and the water stability of the nanosheets, possibly due to increased oxidation of the material (15.4 at.% O).

These results, summarized in table 7, indicate that graphite from discarded batteries has been mostly used to prepare GO nanosheets, yielding materials with similar characteristics to those prepared from common graphite sources. As shown in table 7, impurities are often in not negligible percentage [156, 157, 164] so particular care needs to be taken to purify the final products. Nevertheless, even GO produced by Hummers' method does contain a wide array of impurities in small quantities (ppm range for the most part) [165]. Remarkably, LPE has been hardly investigated: the only work based on shear mixing does report considerably higher C/O ratio, compared to GRMs produced following the GO routes, indicating the possibility to achieve GRMs with low defect concentration in relatively good yield.

2.2.2. Waste graphite

Untreated waste graphite of different morphologies have been used as substitute for commercial graphite powder in the preparation of GO following several variations of Hummers' method with mixed results,

Table 7. Starting materials, preparation steps and characterization of GRMs produced from batteries.

Precursor	Pre-treatment	Treatment	Product	Microscopy	Elemental analysis	Diffraction	Spectroscopy	BET ($m^2\ g^{-1}$)	Yield	References
Graphite rods (Zn–C batteries)	Washing Crushing into powder	Hummers' reduction with hydrazine	GO rGO	Nanosheet	GO: 45.72%C, 49.21% O, 1.56% Al, 3.51% Si rGO: 74.54% C, 24.72% O, 0.48% Al, 0.26% Si	GO peak at 11.54°, rGO at 24.6°	$I_D/I_G = 0.96$ (GO);=0.98 (rGO) **FTIR**: C–O, C=O, C–OH, O–H abs at 237 nm (GO), 272 nm (rGO)			[156]
Graphite rods (Zn–C batteries)	Washing Crushing into powder	Modified Hummers'	GO		Impurities: MnO, Na_2O, SO_3, K_2O, SiO_2, MgO, CaO, Al_2O_3	Main peak at 27°. Impurities of MnO_2, SiO_2	**FTIR**: O–H, C=O, Mn impurities			[157]
Graphite rods (Zn–C batteries)	Washing with water	ECE, 10 V, 0.5 M H_2SO_4, 2 h; 650 °C, 3 h, Ar	GO, rGO	Nanosheet; few- to multilayer	22.8% O, 13.6% after reduction	Broad peak at 26.6° turbostratic layers	$I_D/I_G = 0.95$ (GO)-1.06 (rGO) **FTIR**: O–H, CH_2, C=C, C–O, C–OH, C–O–C peaks	17 (GO) 27 (rGO)	88%	[159]
Graphite rods (Zn–C batteries)	Washing with water	ECE, 3–8 V, 0.001–0.5 M PSS	Graphene	Nanosheet; few- to multilayer		Peaks at 26.5° and 44.75°	$I_D/I_G = 0.86$–0.95 **FTIR**: O–H, C–H, CO_2, C–O, C=O, C=C, C–S peaks			[160]
Graphite powder (Li batteries)	Grinding Washing	Modified Hummers'; 80 °C, 1 h; 300 °C, 1 h	GO, rGO	Nanosheet; few- to multilayer	26.3% O (GO) 17.2% (rGO), 0.4% Si	Peak at 24.6°	$I_D/I_G = 0.93$–1.25	49.6–362.4		[161]
Graphite powder (Li batteries)	Leaching with ammonia	H_2SO_4, $KMnO_4$, 5 h; peroxyacetic acid	rGO	Nanosheet; few- to multilayer	C/O = 1.79		$I_D/I_G = 1.04$–1.05 **FTIR**: C=O, C–C, C–O, C–OH, C-O–C peaks	108.2–114.6		[1]
Graphite powder (Li batteries)	Grinding Washing	Modified Hummers'	GO	Ultrathin nanosheets	63%–66% C, 33%–36% O	Broad peak at 10–12°		135–215		[163]

(Continued.)

Table 7. (Continued.)

Precursor	Pre-treatment	Treatment	Product	Microscopy	Elemental analysis	Diffraction	Spectroscopy	BET ($m^2\ g^{-1}$)	Yield	References
Graphite powder (Li batteries)	Washing	One-step Hummers'	GO	Monolayer	40.4% O, C/O = 1.475			297.8		[164]
Graphite powder (Li batteries)	Washing	Shear mixing pre-treatment with 4 M H_2SO_4, 4 h	Graphene	<7 layers	85.3% C, 11.2% O, 3.5% F, C/O = 7. 62; pre-treated:84% C, 15.4% O, 0.5% F, 0.1% Co, C/O = 5.45	(002) peak at ∼26°	$I_G/I_{2D} = 2$ is there any D peak?	424.9	33%–87%	[164]

owing to the different characteristics of each graphite. González-Barriuso *et al* produced monolayer GO using waste graphite powder and highly oriented pyrolytic graphite (HOPG) as starting materials in a modified Hummers' method: the obtained material had similar features as the ones prepared with commercial graphite powder [166]. Ground graphite foil was used by Barbakadze and co-workers, yielding GO with C/O of 0.62 that could be subsequently reduced with ascorbic acid to produce rGO with a C/O of 4 [167]. Also using a modified Hummers' process, Kusrini *et al* used graphite waste from the spent pot lining of aluminium industry to produce multilayer GO [168]. This material displayed incomplete oxidation (C/O of 6.22) and presented impurities of several elements such as Al, Na, F and Ca, proving the exfoliation conditions were not adequate for the preparation of high quality material. Graphite waste from the diamond industry was used by Ding and co-workers in a modified Hummers' method, yielding few-layer GO with similar properties, as commonly produced GO [169]. In 2019, Tian *et al* employed an improved one-pot Hummers' method using waste toner powder to prepare GO [170]. The final material is comprised of few-layer GO nanosheets and significantly oxidised with a C/O ratio of 1.82, and only 0.1 at.% Fe and 0.2 at.% Si were still present from the starting material. Using a different approach, waste graphite powder was used to prepare S- and N-doped GQDs by Jlassi *et al* in a multi-step procedure [171]. Graphite was treated first with H_2SO_4 and HNO_3 for 12 h at 120 °C, and then with NH_3 at 180 °C for another 12 h. The resulting material was comprised of aggregated 1–10 nm thick GQDs that showed fluorescence emission with a maximum peak at 437 nm. FTIR and XPS analysis showed the O and N functional groups, but no quantitative chemical composition was reported. Lastly, Sankar *et al* used discarded graphite rods from mosquito repellent in an ECE process, using sodium dodecylbenzenesulfonate as electrolyte [172]. The obtained graphene shows the typical D, G and 2D Raman bands and a lamellar morphology, while both XPS and FTIR show that the material is significantly oxidised. No qualitative composition nor a discussion on the material thickness is reported.

Table 8 shows that this strategy seems to be effective for the production of GO based materials. As discussed for the case of batteries, only one work reports the use of ECE for production of graphene. It is clear that more studies need to be conducted based on the use of ECE and LPE in order to evaluate the use of waste graphites for production of pristine graphene.

2.2.3. Coal and oil waste

The first report, to the best of our knowledge, on the use of raw coal waste as precursor is from 2012 [173]. The starting material was graphitized at 2400 °C in the presence of iron, followed by a Hummers' process. The GO obtained in this way was subsequently reduced with H_2 plasma, yielding thin graphene structures. A different approach was taken by Ye and co-workers for the production of GQDs from coal [174]. In this work, the authors sonicated the raw coals in sulfuric and nitric acid mixtures, followed by mild heating at 100 °C–120 °C for 24 h. The resulting product was water-dispersible and oxidised GQDs, with sizes ranging from 2.3 to 2.96 nm and I_D/I_G of 1.55. In 2020, Lawagon and co-workers described the preparation of sulfonated GO using heavy fuel oil as the starting material [175]. To this end, oil was first treated with sulfuric acid for 24 h and heated it to 900 °C in the presence of a Mn salt. The carbonized product was then processed following Hummers' method, and lastly sulfonated using chlorosulfonic acid, yielding a sulfonated GO with a C/O ratio of 0.90 and containing 7.58 at.% S. Using a similar approach, Sahoo *et al* have recently reported the preparation of GO from bio-soot [176]. The residue from diesel engines was collected, washed, sonicated in water and treated with HCl for 24 h, before being used in a modified Hummers' procedure. The resulting GO shows the typical nanosheet and graphitic morphology, with a composition of 94.34 at.% C, 5.66 at.% O, hence indicating a much lower oxidation degree than what is found commonly for GO [46, 47]. Using a high-temperature approach, Yang *et al* produced porous carbon nanosheets from petroleum asphalt [177]. The authors mixed the starting material and NaCl and used ball-milling for 8 h, before heating the product to 800 °C for 1.5 h in Ar atmosphere. The resulting product displayed nanosheet morphology, a high number of defects as shown by its Raman spectrum ($I_D/I_G = 0.92$–0.99), and the presence of C, O, N, and S in its composition. In 2020, Luong *et al* reported the flash Joule heating of a number of carbon sources (i.e. carbon black, anthracite, coke, coffee) to produce graphene structures in grams scale [178]. In their process, the starting materials were placed between two electrodes and electrical current was passed through, causing the temperatures to reach 2227 °C–2727 °C by inducing graphitization. As a result, turbostratic layered structures with lateral sizes of 0.5–1.2 μm were obtained, with varying oxygen contents and defects, depending on the starting materials (∼0–4.4 at.% O).

2.2.4. Waste plastics

Algozeeb *et al* extended the applicability of their process to polymer waste such as polyethylene terephthalate (PET), high-density polyethylene (HDPE), polyvinyl chloride (PVC), low-density polyethylene (LDPE), polypropylene (PP), polystyrene (PS) [179]. The material produced with this method was made of thin (∼4 layers), 16–27 nm wide nanosheets, with variable amounts of defects ($I_D/I_G = 0.03$–0.14) and trace O signals. Other types of polymer waste derived from plastic have also been used in the preparation of graphene, following different thermal treatment

Table 8. Starting materials, preparation steps and characterization of GRMs produced from waste graphites.

Precursor	Pre-treatment	Treatment	Product	Microscopy	Elemental analysis	Diffraction	Spectroscopy	BET ($m^2\ g^{-1}$)	Yield	References
Waste graphite powder, HOPG	—	Modified Hummers', reduction with $NaBH_4$	GO, rGO	∼1 nm thick, <500 × 500 nm^2		Peaks at 12.8º (GO), 24º (rGO)	**FTIR**: O–H, C=O, $C_{(sp2)}$–O and $C_{(sp3)}$–O			[166]
Waste graphite foil	Grinding	Hummers', reduction with ascorbic acid	GO, rGO	Nanosheet	C/O = 1.61 (GO), C/O = 4.26 (rGO)	Peaks at 10.60º, 10.90º (GO), 23.80º (rGO)	**FTIR**: C=O, C=C, C–F, C–O			[167]
Used graphite electrode	Crushing, sieving	Modified Hummers', reduction with Zn	GO, rGO	Thick nanosheets	C/O = 6.22					[168]
Tailing from diamond synthesis	Acid treating, ball milling, sieving	Modified Hummers'	GO	Few-layer GO, some impurities		Peak at 10.05º	**FTIR**: O–H, C–O, C-O–C, C–OH, CH_2, C=C, H_2O	116.6		[169]
Toner powder	—	Improved Hummers'	Graphene oxide hydrogel	Few-layers GO	64.33% C, 35.37% O, 0.1% Fe, 0.2% Si	Peak at 10.06º	I_D/I_G= 0.85 **FTIR**: C=O, C=C, C–OH			[170]
Waste graphite powder	H_2SO_4, HNO_3, 12 h, 120 °C	Mix with NH_3, 180 °C, 12 h	N,S-doped GQDs	1–10 nm thick		Peak at 27º	I_D/I_G= 1.36, **FTIR**: –CH_2, -OH, C=O, C–H, C–O, C–N, N–H Abs peaks at 230 and 320 nm,			[171]
Mosquito repellent graphite rod	Washing with HCl	ECE, 4.75 V, 0.02 M sodium dodecyl benzene sulfonate, 4 h	Graphene	Lamellar morphology		Peak at 12.7º, broad peak at 26.1º	**FTIR**: C=C, O–H, C–OH, C=O, C–O			[172]

procedures in order to transform the structure of the starting materials. In their work from 2014, Gong *et al* pyrolyzed discarded PP at 700 °C in the presence of montmorillonite [180]. After processing, the resulting material was comprised of multilayer graphene sheets (<12 layers) with an I_D/I_G of 1.35 and C/O ratio of 4.88. With a similar strategy, the work of Pandey *et al* made use of bentonite as a template for the pyrolysis of different polymers (i.e. PP, PET, PS) in a two-stage process, at 400 and 750 °C [181]. As a result of this process, few-layer graphene nanosheets with an I_D/I_G of 0.90 were obtained, but no quantitative measurement of their thickness or oxidation was reported. PET derived from plastic bottles was used by El Essawy *et al*, as the starting material in a pyrolysis process [182]. The starting material was heated inside a stainless steel reactor at 800 °C for 1 h, yielding a mixture of graphite and few-layer graphene characterized by I_D/I_G of 1.13 and trace amounts of oxygen. Very recently, Ko and co-workers reported the conversion of PET into graphite and its subsequent exfoliation [183]. The authors carbonized the polymer at 900 °C and then carried out its boron-catalysed graphitization at 2400 °C. Graphite prepared by this method was then treated with a mixture of sulfuric and nitric acids, subjected to a microwave treatment and finally sonicated in NMP, yielding to few-layer graphene nanosheets. Polyamide was used by Stanford *et al* as the starting material for the preparation of laser-induced graphene [184]. The authors irradiated the starting polymer with a pulsed CO_2 laser, promoting its transformation into nanosheet structures that displayed the typical D, G and 2D bands in their Raman spectrum. This polymer was also used by Huang *et al* recently to prepare both GQDs and nanosheets [185]. The material was pyrolyzed at 800 °C–2000 °C and then used in an ECE process with diluted NH_3 as the electrolyte, producing GQDs (1–6 layers thick, 3.9–7.45 nm wide), with a composition of 60–77 at.% C, 12–20 at.% O, 10–20 at.% N and a 98% yield. The authors found that polyimide pyrolyzed at higher temperatures (2300 °C–2800 °C) did not yield GQDs when used in the same procedure, but using $(NH_4)_2SO_4$ in the ECE step yielded graphene nanosheets with a yield of 82%. These nanosheets were found to have single-crystal graphitic structure, but no further characterization was reported. In 2017, Nguyen *et al* annealed Parafilm on Ni meshes at temperatures between 600 °C and 980 °C in vacuum conditions [186]. The resulting hollow fibres were comprised of few-layer graphene (6–8 layers) with low amounts of defects, as evidenced by I_D/I_G of 0.14–0.54, having lower ratios at higher temperature treatments. 3D graphene structures were obtained by Wang and co-workers in 2019 using waste tires as the starting material [187]. In this work, the authors used KOH as the activating agent in a pyrolysis process at 800 °C–100 °C, obtaining interconnected nanosheet structures comprised of few-layer graphene with low amounts of oxygen.

Tables 9 and 10, summarizing the results obtained with the last two approaches, show that thin nanosheets or filaments are typically produced, with an exact elemental composition that depends on the source of carbon and processing used.

3. Environmental impacts of graphene-related materials production processes

As a result of the environmental concerns around the production of nanomaterials, several LCA studies focusing on the environmental impacts of different GRM production processes have emerged in the literature, with the earliest study dating back to 2014 [188, 189]. These studies are listed and summarised in table 11. As can be observed, these studies have looked at few production processes and their variations: chemical oxidation with chemical, biological and thermal reduction using various reduction agents for production of GO and rGO, microwave-assisted exfoliation, LPE, ECE, ball milling exfoliation, CVD, and epitaxial growth. We remark that some of these methods, such as microwave-assisted exfoliation, epitaxial growth or biological chemical reduction are currently not considered as technologies for scalable production of graphene (section 1.2). In the case of GO, in addition to the traditional Hummers' method, other modified approaches have been also considered, such as the Marcano, Fugetsu, Bangal and Jeong methods as well as the first methods used to produce GO by Brodie and Staundenmaier [45, 190–194].

All studies included in this section reported direct contributions from the production of GRMs, however, the system boundaries varied from 'cradle to gate', [188, 195–201] 'cradle to installation' [202] and 'cradle to grave' [189]. The functional unit varied across these studies, with the large majority defined in terms of mass, e.g. *mg*, *g* or *kg* of graphene produced. In the particular case of CVD and epitaxial growth, the functional unit has also been defined in terms of surface area in some studies [197, 198, 200], e.g. cm^2 of graphene. This is because these methods produce graphene monolayers rather than dispersions (see section 1).

The studies considered different types of feedstock for the production of GRMs, including graphitic and non-graphitic, fossil based or renewable sources, e.g. biomass [195]. Other carbon-based precursors, which we have described in the second part, were not considered. Most studies relied on laboratory scale data to conduct the LCA studies for the GRMs. The studies conducted by Ampah *et al* [196] and Cossutta *et al* [200] used simulated commercial scale data based on various assumptions, whilst Arvidsson and Molander [198] used experimental

Table 9. Starting materials, preparation steps and characterization of GRMs produced from coal and oil waste.

Precursor	Pre-treatment	Treatment	Product	Microscopy	Elemental analysis	Diffraction	Spectroscopy	BET ($m^2\ g^{-1}$)	Yield	References
Anthracite coal	Fe, 2400 °C, 2 h, Ar	Hummers'; H_2 DBD plasma treatment	GO, rGO	Nanosheet		Peak at 11°, disappears after plasma treatment	I_D/I_G decreases after reduction. **FTIR**: C=O, C–O, O–H, =C–H, C=C	135–306		[173]
Bituminous coal, coke, anthracite	Sonication in H_2SO_4 and HNO_3, 2 h	100 °C–120 °C, 24 h	GQDs	2.3–2.96 nm size, 1.5–3 nm thick			I_D/I_G = 1.28–1.90 **FTIR**: C–O, C=O, O–H Emission peak at 530, 480, 460 nm		10%–20%	[174]
Heavy fuel oil	H_2SO_4, 180 °C, 24 h; $Mn(NO_3)_2$, 900 °C, 3 h, N_2	Modified Hummers'; Chlorosulfonic acid, 70 °C, 4 h	GO, Sulfonated GO	Few-layers	C/O = 0.79–0.90, 1.54%–7.58% S		I_D/I_G = 0.67–1.06 **FTIR**: C=O, O–H, C–OH, C–O, –SO_3H	181.13–246.18		[175]
Bio-soot	Washing, sonication in water; HCl 24 h	Modified Hummers'	GO	Nanosheet	94.34% C, 5.66% O	Peaks at 10.8, 43.5°	**FTIR**: C=C, C=O, COOH, C–OH	82		[176]
Petroleum asphalt	Mixing with NaCl, ball milling 8 h	800 °C, 1.5 h, Ar	Porous carbon nanosheets	Nanosheet			I_D/I_G = 0.92–0.99	5.28–23.6		[177]
Carbon black, anthracite, coke, coffee	—	Flash Joule heating	Graphene	Layered, turbostratic structure. 0.5–1.2 μm lateral size.	95.6%–100% C, 0%–4.4% O	Peak at 26.1°	I_D/I_G = ∼0.0–1.4	∼295	35%–90%	[178]

Table 10. Starting materials, preparation steps and characterization of GRMs produced from waste plastics.

Precursor	Pre-treatment	Treatment	Product	Microscopy	Elemental analysis	Diffraction	Spectroscopy	BET ($m^2\ g^{-1}$)	Yield	References
PET, HDPE, PVC, LDPE, PP, PS	Mix with carbon black	Flash Joule heating	Flash graphene	16–27 nm size sheets, four-layer thick		Peaks at 26.1º, 45º	$I_D/I_G = 0.03$–0.14		Up to 30%	[179]
PP from bumper	Grinding into granules	700 °C mixed with organically modified montmorillonite	Graphene flakes	Nanosheet morphology, up to several μm in lateral size	C/O = 4.88	Peaks at 24.6º, 43.0º	$I_D/I_G = 1.35$–2.27		14.6–86.6%	[180]
Plastic (PP, PE, PS)	Crushing, washing, mixing with bentonite nanoclay	Pyrolysis (N_2, 400 °C, then 750 °C). Washing with HCl to remove bentonite.	Graphene nanosheets	Wrinkled nanosheets	76.99% C, 21.1% O	Peaks at 7º, 27º and 50º	$I_D/I_G = 1.11$ **FTIR**: C–O, C–O–C, O–H, CH_2, C=C, C=O			[181]
PET from bottles	Crushing, sieving	800 °C, 1 h	Graphene	Fiber network morphology; few-layer graphene		Peaks at 26, 42.3 and 44.3º	$I_D/I_G = 1.13$ **FTIR**: O–H, C=O, C–O–C, C–O	721.7		[182]
PET from bottles	900 °C, 1 h, N_2; Boron, 2400 °C, 1 h, He	H_2SO_4, HNO_3, 24 h; Microwave treatment; Sonication in NMP	Graphene sheets	Lateral size of 410 nm, few-layers		Peaks at 26º, 43º, 77.2º and 83.3º				[183]

(Continued.)

Table 10. (Continued.)

Precursor	Pre-treatment	Treatment	Product	Microscopy	Elemental analysis	Diffraction	Spectroscopy	BET ($m^2\ g^{-1}$)	Yield	References
Polyimide	—	75 W pulsed CO_2 laser	Laser-induced graphene	Nanosheet filaments						[184]
Polyimide	800 °C –2000 °C pyrolisis	ECE, 3–30 V, 0.05 M NH_3, 2 h	GQDs	3.9–7.45 nm size; 1–6 layers	60%–77% C, 12%–20% O, 10%–20% N		$I_D/I_G = 2$		98%	[185]
Polyimide	2300 °C–2800 °C pyrolisis	ECE, 5 V, 1 M $(NH_4)_2SO_4$	Graphene	Nanosheet					82%	[185]
Parafilm	Washing, drying	600 °C–980 °C, 8 min, vacuum on Ni mesh	Hollow few-layer graphene fiber mesh	6–8 layers		Peak at 26.5°	$I_D/I_G = 0.14$–0.54 **FTIR**: C–C–O, C–O/OH, C=O, C=C			[186]
Tires	Grinding, mixing with KOH	800 °C /900 °C /1000 °C, 2 h	3D graphene	Up to several μm in lateral size, 3.5–4 nm thick (few-layer)	82.1%–92.6% C, 4.8–9.2% O, 0.4%–1.4% S, 0.1%–0.9% H, <0.1% metals	Peaks at ∼26°, ∼44°, ∼46°	$I_D/I_G = 0.21$-1-26	288.6–807.9		[187]

Table 11. Summary of LCA studies on GRM production processes included in this review.

Graphene product, structure and application	Carbon feedstock	Production process	Functional unit	System boundaries	Scale	Environmental impacts considered (method)	References
3D graphene foams (3DGF)	Biomass and methane	Rapid pyrolysis Atmospheric-pressure; CVD and Conventional CVD	1 kg of 3DGF	Cradle to gate	Laboratory	18 midpoint categories (ReCiPe), e.g. CC and CED	[195]
Graphene back contacts for PV devices	Methane	CVD	151 kg of graphene	Cradle to installation	Laboratory	9 midpoint categories (TRACI 2.0), e.g. GWP	[202]
Graphene and graphene ink (heating element)	Graphite from coke and coal tar	Sulphuric acid used as pretreatment, microwave assisted exfoliation	0.95 kg of graphene; 3.2 kg graphene ink	Cradle to gate	Commercial	Embodied energy	[196]
Graphene (surface) layers for transparent electrodes, e.g. LCDs, PVs	Methane	CVD	1 cm^2 of graphene	Cradle to gate	Laboratory	Life cycle energy use (CED) and scarce metals (EPS 2000)	[197]
Reduced graphene sheets	Graphite	Chemical oxidation/ chemical reduction (Hummers' process, hydrazine and *E. coli* as reduction agents)	1 kg of graphene	Cradle to gate	Laboratory	10 or 11 midpoint categories (CML), e.g. GWP, ADP fossil	[199]
Reduced graphene (unorganised nanoplatelet and sheets for bulk applications, and single monoatomic layer for planar applications)	Graphite	Chemical oxidation/- chemical and thermal reduction (various methods); ECE; CVD	1 g of graphene; 1 cm^2 of graphene (CVD)	Cradle to gate	Laboratory and commercial (simulation)	13 midpoint categories (ILDC), e.g. GWP	[200]

(Continued.)

Table 11. (Continued.)

Graphene product, structure and application	Carbon feedstock	Production process	Functional unit	System boundaries	Scale	Environmental impacts considered (method)	References
Surface layers of graphene	Coke	Epitaxial growth	1 cm^2 of graphene	Cradle to gate	Laboratory, pilot (real data) and industrial (hypothetical)	CED, CC, terrestrial acidification, freshwater ecotoxicity and ecotoxicity (ILCD)	[198]
Graphene in solution (sheets >100 nm and 1–10 nm). Bulk applications, e.g. composite additives	Graphite from hard coal	Chemical oxidation/chemical reduction (Hummers' process and Marcano's modification), and LPE	1 kg of graphene in solution	Cradle to gate	Laboratory	Energy use, blue water footprint, human toxicity and ecotoxicity (ILCD)	[188]
Reduced graphene thin films for bulk applications and monolayers for electronic applications	Graphite	Chemical oxidation/-chemical reduction (Hummers'process and Marcano's modification, with hydrazine and glucose as reduction agents)	1 kg of graphene; mg S^{-1} m^{-1}	Cradle to gate	Laboratory	16 midpoint categories (ILCD), e.g. GWP, CED, toxicity	[201]
Epoxy-based nanocomposites, filled with graphite nanoplatelets[c]. Heat sinks in electric or electronic systems.	Graphite	Sulphuric acid pretreatment, exfoliation is microwave assisted (thermal exfoliation)	1 kg of epoxy nanocomposite	Cradle to grave	Laboratory	13 midpoint categories, e.g. GWP (IPCC), energy consumption (CED), others (ReCiPe, CML, EDIP, USEtox)	[189]
Graphene and few layer nanosheets for bulk applications.	Graphite	Ball milling exfoliation with and without use of melamine as exfoliating agent	1 mg of graphene in solution	Cradle to gate	Laboratory	15 midpoint categories (ILCD), e.g. CC and CED; 4 endpoint damage levels (IMPACT 2002+)	[203]

and commercial data at laboratory and pilot scale and a hypothetical industrial scale scenario based on what-if assumptions.

The environmental impacts were assessed using different LCA methods including CML, ReCiPe, TRACI and ILCD. The number of environmental impact categories included varied across studies, with GWP and energy demand, e.g. cumulative energy demand (CED), process energy, being consistently assessed in most studies. Therefore, this section will discuss and compare GWP and energy demand results reported in these studies, which are presented in figures 8 and 9, respectively. Given that GWP can be directly associated with embodied energy estimations, e.g. reactants, and process energy consumption, assuming these are sourced from fossil fuels, their combined analysis can help identifying clearer environmental sustainability trends amongst production processes. The variations in GWP and energy demand observed for each production process are due to various factors including methods employed, structure of GRMs and scale considered, and will be discussed in detail over the next sections.

3.1. Chemical oxidation with chemical and biological reduction

The studies conducted by Khanam *et al* [199], Cossutta *et al* [200], and Serrano-Luján *et al* [201] assessed the production of GRMs from graphite, and Arvidsson *et al* [188] from hard coal using the chemical oxidation with chemical reduction process. Khanam *et al* [199] also looked at microbial reduction using *E. coli*. All studies reported GWP and/or energy demand results on a mass basis and are presented in figures 8(a) and 9(a), respectively. As it can be observed in figure 8(a), there is a large variation in the GWP results reported in these studies. One of the reasons behind this is the different graphite oxidation methods used, e.g. Hummers' or modified methods (referred as: Marcano's, Brodie, Staundenmaier), and the reduction agents employed, e.g. hydrazine, glucose, *E. coli*. In the case of the Hummers' method using hydrazine as the reducing agent, the GWP is reported at 586 kg CO_2 eq. kg^{-1} graphene, with the production and use of hydrazine and phosphoric acid identified as the main hotspots [201]. When using glucose as the reducing agent, Serrano-Luján *et al* [201] found that the GWP of this process reduces by 40% (343 kg CO_2 eq. kg^{-1} graphene). The GWP associated to some modified versions of the Hummers' method are reported by Cossutta *et al* [200] at 153 kg CO_2 eq. kg^{-1} graphene, 146 kg CO_2 eq. kg^{-1} graphene and 380 kg CO_2 eq. kg^{-1} graphene for the Fugetsu, Bangal and Jeong modifications, respectively. These modifications, which have been reported to improve the oxidation efficiencies of the process via temperature and acid ratios tuning, [200, 201] offer significant GWP reductions as well (35%–73%) with respect to the original Hummers' method using hydrazine. The large GWP difference observed between the Fugetsu and Bangal methods with the Jeong method is due to the higher amounts of sulphuric acid employed in the latter [200]. Cossutta *et al* [200] also looked at the Brodie and Staundenmaier methods, which resulted in a GWP of 207 kg CO_2 eq. kg^{-1} graphene and 210 kg CO_2 eq. kg^{-1} graphene, respectively. Besides graphite consumption, these studies have identified the chemical inputs and the acid neutralisation step as the main hotspots of this production process, whilst energy consumption was found to be a minor contributor. The oxidative agents used across these methods also contributes to the differences in GWP reported. For example, the Hummers' method and its modifications used potassium permanganate, which has a GWP of around 1.78 kg CO_2 eq. kg^{-1}, [83] whilst the Brodie method uses sodium chlorate [83] (4.96 kg CO_2 eq. kg^{-1}) and the Staundenmaier method employs potassium chlorate [83] (around 7 kg CO_2 eq. kg^{-1}), which have higher environmental burdens associated with their production processes [200, 201]. From all the methods reported here, the Bengal modification of the Hummers' method has the lowest GWP mostly because it uses potassium permanganate as the oxidative agent, employs less acid and the process is carried out under 30 min at 35 °C, thus minimising energy requirements [200].

Another factor contributing to the large difference observed across GWP results reported in the literature and as shown in figure 8(a), is the structure of the GRM obtained and the intended application. For example, the studies previously discussed looked at the production of thin-films [201] and nanoplatelets [200] of graphene for bulk applications, which ranged between 146 and 586 kg CO_2 eq. kg^{-1} graphene.

Khanam *et al* [199] studied the production of graphene sheets using the Hummers' method with hydrazine as the reducing agent, and reported a GWP of 85 kg CO_2 eq. kg^{-1} graphene. The final application of the GRM was not specified in the study, and whilst this is the lowest value reported for this production process using laboratory scale data, there is not enough information available to help explain such difference with respect to other studies. The scale of the process, and therefore the data and assumptions made, also contributes significantly to the differences observed. For instance, Cossutta *et al* [200], which used simulated process data at a commercial scale, reported one of the lowest GWP results observed for chemical oxidation with chemical reduction at 81 kg CO_2 eq. kg^{-1} graphene, which is 4 times lower than the average GWP results based on laboratory scale date for this process [199–201]. Khanam *et al* [199] also considered chemical oxidation via the Hummers' method with biological reduction using *E. coli* as the reducing agent, and reported a GWP of 60 kg CO_2 eq. kg^{-1} graphene. The conversion

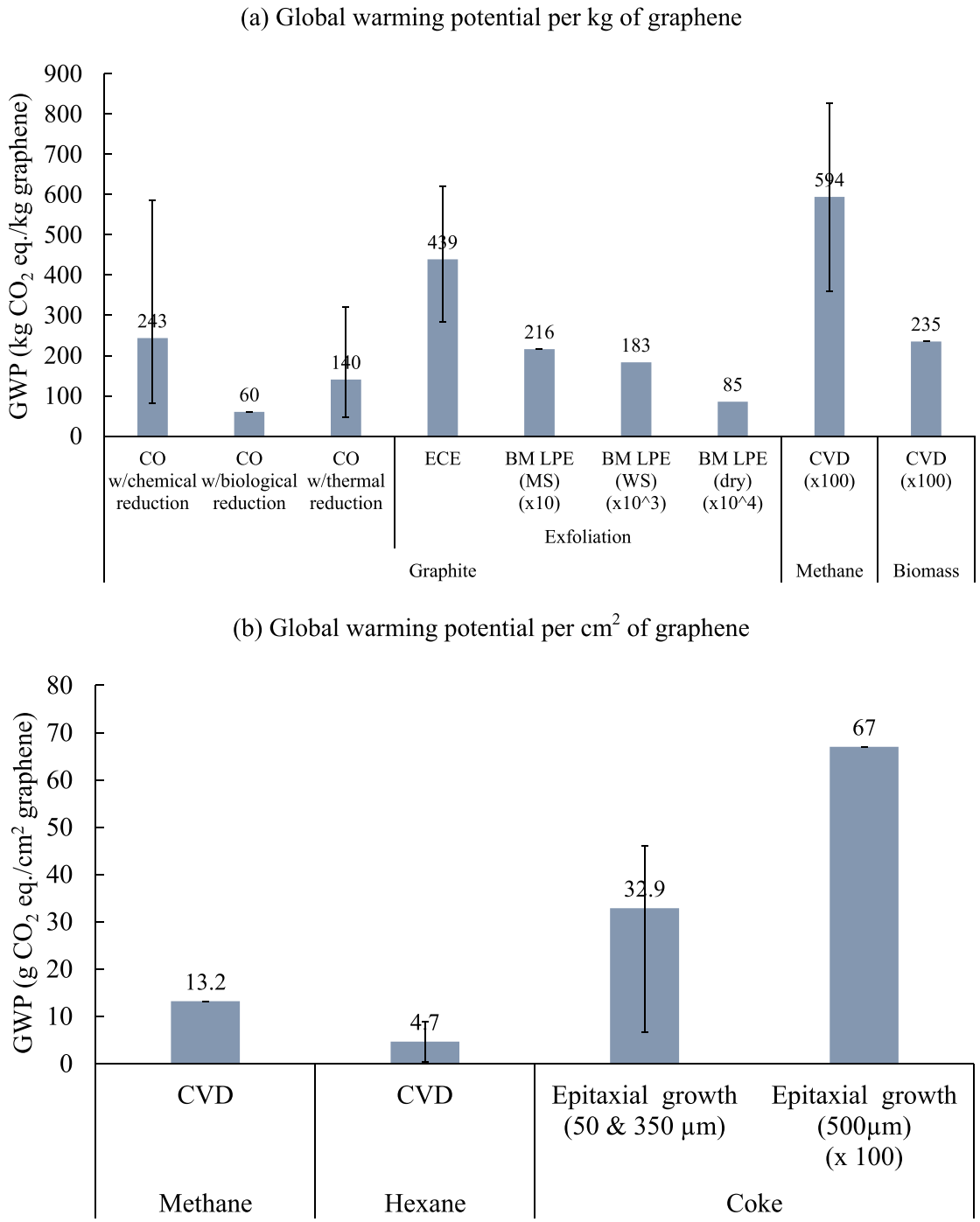

Figure 8. GWP of graphene expressed (a) per kg graphene and (b) per cm^2 graphene [195, 198–203]. Average GWP values are displayed and the error bars indicate the ranges reported in the studies included here. The values of some production processes have been scaled to fit. The original values can be obtained by multiplying the value shown on top of the bars by the scaling factor given on the *x*-axis. Ball milling (BM) results are reported in melamine solution (MS), water solution (WS) and on a dry basis. Epitaxial growth results are reported in terms of the SiC wafer thickness. CO: chemical oxidation; ECE: electrochemical exfoliation; LPE: liquid phase exfoliation; CVD: chemical vapour deposition.

process occurs at room temperature thus reducing the energy requirements of the process. Serrano-Lujan *et al* [201], Arvidsson *et al* [188] and Khanam *et al* [199] also assessed the energy demand for the production of GRMs via chemical oxidation and reduction. Whilst a direct comparison of the results is not possible as the studies employed different methodologies (see figure 9(a)), all three studies concluded that the chemical reduction step is energy intensive and was identified as the main hotspot for this process. For example, Serrano-Lujan *et al* [201] estimated the CED of the GRMs and reported values of 33 470 and 38 150 MJ kg^{-1} graphene for the Hummers' method using glucose and hydrazine, respectively, with process electricity consumption contributing with 80%–95% of the total CED (see figure 9(a)). Arvidsson *et al* [188] estimated the heat and electricity requirements of the GRM production process using the Hummers'

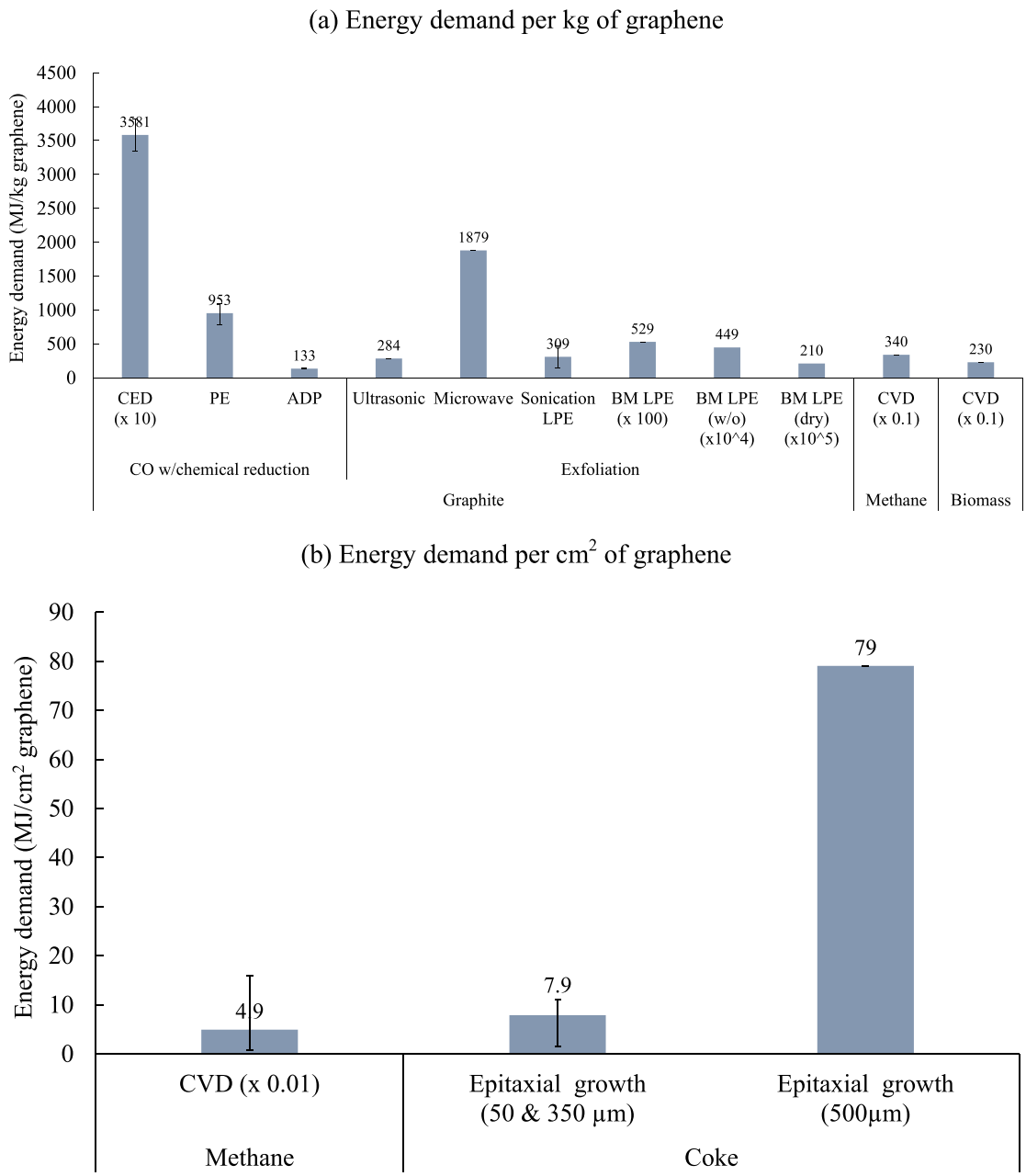

Figure 9. Energy demand of graphene production expressed (a) per kg graphene and (b) per cm^2 graphene [188, 189, 195–199, 201, 203]. Average energy demand values are displayed and the error bars indicate the ranges reported in the studies included here. The values of some production processes have been scaled to fit. The original values can be obtained by multiplying the value shown on top of the bars by the scaling factor given on the *x*-axis. Ball milling results are reported in melamine solution, water solution (w/o) and on a dry basis. Epitaxial growth results are reported in terms of the SiC wafer thickness. CO: chemical oxidation; LPE: liquid phase exfoliation; CVD: chemical vapour deposition. Cumulative energy demand (CED); process energy (PE), abiotic depletion potential (ADP).

method and the Marcano's modification, and the results are included in figure 9(a). The study found that the Hummers' method requires 1100 MJ kg^{-1} graphene, which is around 25% more energy consumption compared to the Marcano's method estimated at 780 and 980 MJ kg^{-1} graphene, depending on the amount of oxidative agent used. The heating requirements of the chemical reduction stage and hydrazine production were identified as the main hotspots for these processes [188]. Khanam *et al* [199] assessed the abiotic depletion potential of fossil energy for the studied GRMs production routes, and the results varied slightly depending on the reduction agent used, 139.38 MJ kg^{-1} graphene for hydrazine and 127.26 MJ kg^{-1} graphene for *E. coli*. The study also identified the heating requirements for the chemical reduction as the main hotspot, and the production of hydrazine accordingly.

Based on these findings, the selection of oxidative and reducing agents can play an important role in reducing the total GWP and energy demand of GRMs produced using chemical oxidation and reduction. Moreover, the scaling up of this production process also offers ample room for improvement through

higher energy efficiencies and higher acid recovery rates.

3.2. Chemical oxidation with thermal reduction

The GWP results for chemical oxidation with thermal reduction presented in figure 8(a) correspond to the study by Cossutta *et al* [200]. The study compared five GO production methods from graphite with thermal reduction carried out under the same conditions at laboratory and commercial scale. The chemical oxidation methods included three modifications of the Hummers' method (Fugetsu, Bangal and Jeong) and the Brodie and Staundenmaier methods. The GWP values for this production process ranges from 86 to 320 kg CO_2 eq. kg^{-1} graphene at laboratory scale, were the Bangal and the Jeong modifications of the Hummers' method have the lowest and highest GWP, respectively. The reported GWP of the Bangal method at the commercial scale (46 kg CO_2 eq. kg^{-1} graphene) is 46% lower compared to the results estimated at laboratory scale due to potential improvements based on experimental insights around energy efficiency and material recovery. The GWP of chemical oxidation with thermal reduction is between 16%–40% lower compared to the results reported for chemical reduction discussed in section 2.1, as this method requires less chemicals.

3.3. Chemical exfoliation (electrochemical, ultrasonic, microwave assisted and ball milling)

The studies conducted by Cossutta *et al*, [200] Ampah *et al*, [196] Pizza *et al* [189], Arvidsson *et al*, [188] and Beloin-Saint-Pierre and Hischier [203] assessed the production of GRMs using different exfoliation techniques from graphite. Cossutta *et al* [200] estimated the environmental impacts for the production of graphene sheets via ECE, including GWP results. Ampah *et al* [196] and Pizza *et al* [189] reported energy consumption values for the production of GRMs using both expansion and ultrasonic exfoliation and microwave-assisted exfoliation. In the case of Ampah *et al*, [196] the study looked at the production of graphene ink to make coatings for heat management, whilst Pizza *et al* [189] considered the production of epoxy-based nanocomposites using graphite nanoplatelets as fillers. Both studies focused on the energy requirements for the production of GRM components. Ampah *et al* [196], Arvidsson *et al* [188] and Beloin-Saint-Pierre and Hischier [203] looked at variations in ultrasonic-assisted exfoliation for the production of GRMs using different solvents as exfoliation agents. Ampah *et al* [196] and Arvidsson *et al* [188] reported the energy demand of the production of GRMs using sonication and dimethyl formamide and dimethyl ether as exfoliating agents, respectively. Beloin-Saint-Pierre and Hischier [203] assessed a ball milling process for the production of GRMs in water with and without using melamine as the exfoliating agent and reported values for GWP and CED, among other environmental impacts.

The GWP of graphene produced using ECE ranges between 330 and 620 kg CO_2 eq. kg^{-1} graphene according to the study conducted by Cossutta *et al* [200], where different set of electrolytes (sodium acetate and potassium hydroxide) and operating conditions (9 and 15 V) were considered at laboratory scale. These results are presented in figure 8(a). It was observed that energy efficiency increases with higher applied potential for both electrolytes, however, the use of the potassium hydroxide electrolyte at 15 V resulted in the highest energy efficiency and therefore was reported to have the lowest GWP at 330 kg CO_2 eq. kg^{-1} graphene. Electricity consumption was identified as the main hotspot and the contributions from the production of the electrolyte were reported to be negligible. Whilst scaling up the technology to a commercial scale can offer further GWP reductions due to energy efficiency improvements, the study reported a reduction of around 14% (284 kg CO_2 eq. kg^{-1} graphene) with respect to the best performing scenario. This is because the process energy consumption is assumed to be driven by resistance losses, which remain constant at different production capacities of the process.

Beloin-Saint-Pierre and Hischier [203] reported a GWP of 2160 kg CO_2 eq. kg^{-1} graphene for the production of GRMs in melamine solution using a ball milling process, as shown in figure 8(a). The large majority (97%) of this impact is attributed to electricity consumption in the process, which is a lengthy one. For example, for the preparation of 1 mg of graphene, the mixture of graphite and melamine is milled for over 30 min followed by sonication. The study also looked at the removal of melamine via dialysis to produce a GRM in water solution (with traces of melamine) and the production of GRM powder (dry) using a freeze-drying process, which increased the GWP results significantly due to the additional electricity consumption of such steps. These were reported at 183 000 kg CO_2 eq. kg^{-1} graphene in water solution and 854 000 kg CO_2 eq. kg^{-1} graphene powder.

The energy demand results for the production of graphene using expansion with strong acids and exfoliation by microwave are presented in figure 9(a), and these are reported at 284 MJ kg^{-1} graphene for ultrasonic exfoliation [196] and 1879 MJ kg^{-1} graphene for microwave assisted exfoliation [189]. Whilst the expansion processes reported in both studies requires heat, [189, 196] the large majority of the energy demand is attributed to the exfoliation process. However, the significant difference observed between the two studies with microwave assisted exfoliation consuming five times more energy compared to the ultrasonic exfoliation process. This is because the microwave exfoliation process was carried out over

3 h [189], whilst the ultrasonic exfoliation was completed under 30 min [196].

The energy demand between the sonication and ball milling processes varied significantly as shown in figure 9(a). For example, the average energy demand values reported in Ampah *et al* [196] and Arvidsson *et al* [188] are 148 MJ kg^{-1} graphene and 470 MJ kg^{-1} graphene, respectively, whilst the ball milling process was reported to consume between 52 900 MJ kg^{-1} graphene and 21 000 000 MJ kg^{-1} graphene, depending on the graphene state [203]. Both studies identified the use of solvents as hotspots, whilst the electricity consumption of the sonication process were negligible in comparison. In the case of Ampah *et al* [196], the production of graphene contributed 57% of the total energy demand, followed by the use of dimethyl formamide accounting for 43% of the total energy demand. In the case of Arvidsson *et al* [188], nearly 100% of the total energy demand was attributed to the production and use of the solvent dimethyl ether, as the study assumed no solvent recovery. However, a sensitivity analysis that considered 90% solvent recovery indicated that around 90% of the energy demand could be potentially reduced. As for the ball milling process, electricity consumption was reported as the main hotspot for all processes, contributing with >98% of the total energy demand for the reasons previously discussed.

We remark that the exfoliation by ultrasonication reported in Arvidsson *et al* [188] does not actually correspond to traditional LPE, which requires several days exfoliation of pristine graphite and it is usually performed in organic solvents such as N-methyl-2-pyrrolidone, as discussed in section 1.2. The values reported in Arvidsson *et al* [188] does refer to 30 min sonication in diethyl ether: this solvent does not have suitable properties to efficiently exfoliate graphite [39], hence it has been hardly used for LPE.

3.4. Chemical vapour deposition

The GWP of the production of GRMs using CVD was studied by Zhang *et al* [195], Scott and Cullen [202], and Cossutta *et al* [200], and the energy demand of this process was reported in Zhang *et al* [195] and Arvidsson *et al* [197]. With the exception of Zhang *et al* [195] which studied the production of 3D graphene foams, all studies looked at the production of graphene as conductive layer [197, 202]. The studies considered methane, [195, 197, 200, 202] hexane, [200] and biomass pyrolysis gases, [195] as the precursor gases. The studies conducted by Zhang *et al* [195] and Scott and Cullen [202] used a mass based functional unit and the corresponding GWP and energy demand results are compared in figures 8(a) and 9(a), respectively. Cossutta *et al* [200] and Arvidsson *et al* [197] reported their findings per surface area and are presented in figures 8(b) and 9(b), accordingly.

The GWP reported per kg of graphene are presented in figure 8(a), and the results for GRM derived from methane are reported at 36 000 kg CO_2 eq. kg^{-1} graphene [195] and 82 800 kg CO_2 eq. kg^{-1} graphene [202]. The combustion of natural gas and the use of hydrogen gas were reported in both studies as the main hotspots for this process. The large difference observed between studies can be attributed to various factors including the GRMs structures considered, e.g. 3D foams vs monolayers, the overestimation of natural gas needed reported in Scott and Cullen [202] as well as the inconsistencies in the system boundaries of the studies. For example, Scott and Cullen [202] also considered the transportation and installation in the framework of a specific application of graphene in photovoltaics. The GWP for graphene derived from biomass is estimated at 23 500 kg CO_2 eq. kg^{-1} graphene, which is 35% lower than graphene derived from methane according to the results reported in Zhang *et al* [195], because some of the energy requirements were sourced internally from the thermal energy of pyrolytic gases [195]. This trend is also observed in the total energy demand results reported in Zhang *et al* [195] and presented in figure 9(a). The total energy demand of CVD when using biomass pyrolysis gases is reported at 23 MJ kg^{-1} graphene, which is 32% lower compared to the CED reported for methane.

Figure 8(b) shows the GWP reported per cm^2 of graphene, which corresponds to the results reported in Cossutta *et al* [200]. The study considered methane (1035 °C) and hexane (960 °C) as precursors gases with the process carried out under different furnace temperatures. The GWP reported at laboratory scale are 13.2 g CO_2 eq. cm^{-2} graphene for methane and 8.9 g CO_2 eq. cm^{-2} graphene for hexane. The hexane based process was also assessed at a hypothetical commercial scale assuming adiabatic conditions with a 90% heat transfer efficiency. The results were reported at 0.441 g CO_2 eq. cm^{-2} graphene, which is 20 times lower compared to the GWP at laboratory scale, thus demonstrating the improvement opportunities available through scaling up. The energy demand results reported in Arvidsson *et al* [197] and presented in figure 9(b), are estimated at 0.022 MJ cm^{-2} graphene, with methane production and the process energy during the CVD identified as the main hotspots and these activities contributed with 68% and 15% of the total energy consumption, respectively. The study also considered various scenarios around methane consumption including low residence time, high recovery of methane and a higher methane application rate. Whilst lower residence times and higher recovery rates reduced the total energy consumption by 63% each, higher applications rates were reported to have an energy consumption seven times higher compared to the base case. A hypothetical large scale scenario was proposed based on the combination of the two best scenarios, i.e. lower residence

times and higher recovery rates, with a total energy consumption of 0.0066 MJ cm^{-2} graphene. The study demonstrates that through more efficient consumption of raw materials at larger scales, the CVD process can reduce its energy demand by around 70%. [197].

According to these results, the environmental sustainability of GRMs produced via CVD can be significantly improved through higher heat transfer efficiencies and more efficient consumption of precursor gases. The use of precursor gases derived from renewable feedstock such as biomass can significantly improve the performance of this process.

3.5. Epitaxial growth

Arvidsson and Molander [198] assessed the GWP and energy demand, among other environmental impacts, of GRM produced via epitaxial growth for planar applications, e.g. semiconductors and biosensors, and to date, this is the only study available for this production process. The GWP and energy demand results, which are reported per cm^2 of graphene, are shown in figures 8(b) and 9(b), respectively.

The epitaxial growth process is reported as an energy intensive process as large quantities of electricity are required for the sublimation of the silicon carbide (SiC) powder, e.g. between 1000 °C and 2600 °C depending on the process, and the SiC wafer production processes [198]. The study looked at laboratory, pilot and industrial scale production scenarios from silica sand and coke, using experimental data and hypothetical assumptions in the case of industrial scale. The study considered two scenarios for each production scale based on the thickness of the SiC wafer. A worst case scenario considered SiC wafers with a thickness of 500 μm for all scales, which is the thickness currently manufactured, and a best case scenario assuming a SiC wafer with a thickness of 350 μm for the laboratory and pilot scale, and 50 μm for the industrial scale according to potential technology improvements [198].

The GWP of the worst case is reported at 6700 g of CO_2 eq. cm^{-2} graphene for all scales (500 μm), and for the best case this is 6.6 g of CO_2 eq. cm^{-2} graphene for the industrial scale (50 μm) and 46 g of CO_2 eq. cm^2 graphene for the laboratory and pilot scale (350 μm), as shown in figure 8(b). The main hotspot identified in both cases was the electricity consumption for the production of the SiC wafer. For example, it was reported that this stage contributes over 99% (for the worst case) and 76% (for the best case) to the total GPW. Therefore, the large difference in GWP between the worst and best case is mainly due to the thickness of the SiC wafer.

The energy demand results are presented in figure 9(b), and similar to GWP, it can be observed that the energy demand of the process depends on the different SiC wafer thicknesses. For example, when using a SiC wafer with a thickness of 500 μm, the energy demand is reported at 79 MJ cm^{-2} graphene for all scales, whilst for a thickness of 350 μm the energy demand is estimated at 11 MJ cm^{-2} graphene for the lab and pilot scale, and for the 50 μm thickness assumed for the industrial scale this is 1.6 MJ cm^{-2} graphene. The electricity consumption of the SiC wafer was identified as the main hotspot as it contributes with over 95% of the total energy demand for all scales and scenarios [198].

The study demonstrates that improvements in technology maturity and scaling up of the process can lead to GWP and energy demand reductions of around 85% according to the results reported for the best case scenario. However, given that epitaxial growth relies on energy intensive processes for the production of SiC wafers, the use of renewable electricity, e.g. wind, solar, will play a significant role in the improvement of the GWP of this GRM production process.

4. Outlook

This review shows that one of the most used approaches to deal with environmental harm within graphene production is based on the use of waste material from different sources (section 2). From our review, it is clear that at present there is no suitable approach for the production of high quality graphene from waste material, despite many different processes investigated. The majority of GRMs prepared from waste sources have fairly high amounts of defects, contamination and oxidation, and sometimes not even 2D morphology, which may limit their applications in different fields. These limitations are mainly due to the starting carbon containing waste.

Due to the different starting materials utilized and the diverse treatment processes that the raw waste underwent, a fair comparison among the different presented literature is not possible. In general, amongst waste materials, graphitic waste materials have proven to be the easiest to process and exfoliate, and their characterization often allows one to draw direct comparisons to commonly prepared GRMs. However, residual contamination is still a concern [170]. Non-graphitic waste materials are much more abundant and possess lower value, and thus the interest in their use is higher. From the non-graphitic sources, plant- and animal-derived waste look like the more promising starting materials. This type of waste is abundant, widespread and has low value , often being a cost to be disposed of or recovered through combustion for electricity and heat purposes. Notably, plant-derived wastes contain high quantity of polysaccharides (e.g. cellulose, lignin) that make these precursors suitable for the graphitization processes. It is also important to underline that the majority of the carbon containing waste from biological or non- biological sources investigated so far are well 'defined', i.e. not mixed or blended with other wastes

or contaminated, causing the yield and quality of the product to worsen. Notably, if the route of producing sustainable GMBs is pursued, the waste needs to be well defined and not mixed with other carbon-free waste. For example, the quantity of nitrogen in the initial material needs to remain below 10% or the waste will not pyrolyze properly under thermal treatment. Other sources of contamination (S, P, etc) need to be also controlled and if possible removed/reduced before the transformation processes. The LCA analysis (section 3) shows that the use of waste materials as carbon sources constitutes a rather small part of the whole process; one should also consider the energy cost of high-temperature treatments, the scarcity, cost and environmental impact of reagents and solvents involved in the preparation and processing in order to establish adequate green methodologies. In particular, the LCA results show that the GWP and energy demand of these production processes can vary significantly depending on the choice of reactants, solvents used and operating conditions. The LCA analysis shows that amongst all production methods, the CVD growth can be easily optimized to minimize its energy consumption and GWP values, for example by using biomass gas [195], and by lowering the residence times and increasing gas recovery rates [197]. We remark however that the majority of the LCA studies of GRMs to date are based on laboratory scale data and the interpretation of the results is also strongly dependent on the final application for which the LCA has been performed. Furthermore, LCA has never been applied to graphene produced by LPE, which is one of the most attractive production routes of solution-processed graphene. Despite this, the findings from the prospective studies on LCA of GRMs can still be used to establish performance benchmarks within and across processes, identify opportunities for improvement, quantify potential improvements due to technology maturity or even identify the technological improvements needed to enhance their performance and consequently advanced their commercialisation.

In order to fully exploit the benefits of the LCA methodology, it is recommended for material scientists to work closely with LCA experts in order to use robust data, as done by Beloin-Saint-Pierre D and Hischier [203], to analyze data based on realistic use of a GRM and to make useful comparisons in term of sustainability between different GRMs production routes and related applications. This is particularly relevant for GRMs, as each material in this family has properties suitable for different applications. To give an example, it is unlikely that GO will be used in electronics, so an LCA with focus on GO production for electronics is unlikely to be relevant. Furthermore, despite the numerous works published on sustainable production, none of the LCA works available to date have analysed any of these 'sustainable' approaches.

In conclusion, this review provides an overview on the sustainable routes for production of graphene and related LCA studies, which can be used by the research community to improve the production and the use of GRMs by enabling graphene production to be compatible with the circular economy principles.

Data availability statement

All data that support the findings of this study are included within the article (and any supplementary files).

Acknowledgments

J M and C C acknowledge the EPSRC for financial support (Project EP/P00119X/1). C C also aknowledges support by the Graphene Flagship Core 3 program (Grant Number 881603). C S would like to acknowledge the Italian Ministry of Education, Universities and Research (Ministero dell'Istruzione, dell'Università e della Ricerca—MIUR) through the 'Rita Levi Montalcini 2018' Fellowship (Grant Number PGR18MAZLI).

Conflict of interest

There are no conflicts to declare.

ORCID iD

C Casiraghi https://orcid.org/0000-0001-7185-0377

References

[1] Campanale C, Massarelli C, Savino I, Locaputo V, Uricchio V F and Detailed Review A 2020 A detailed review study on potential effects of microplastics and additives of concern on human health *Int. J. Environ. Res. Public Health* **17** 1212

[2] Chen G, Feng Q and Wang J 2020 Mini-review of microplastics in the atmosphere and their risks to humans *Sci. Total Environ.* **703** 135504

[3] Wang W, Gao H, Jin S, Li R and Na G 2019 The ecotoxicological effects of microplastics on aquatic food web, from primary producer to human: a review *Ecotoxicol. Environ. Saf.* **173** 110–7

[4] Novoselov K S, Jiang D, Schedin F, Booth T J, Khotkevich V V, Morozov S V and Geim A K 2005 Two-dimensional atomic crystals *Proc. Natl Acad. Sci. USA* **102** 10451

[5] Novoselov K S, Fal'ko V I, Colombo L, Gellert P R, Schwab M G and Kim K 2012 A roadmap for graphene *Nature* **490** 192–200

[6] Ferrari A C *et al* 2015 Science and technology roadmap for graphene, related two-dimensional crystals, and hybrid systems *Nanoscale* **7** 4598–810

[7] Döscher H, Schmaltz T, Neef C, Thielmann A and Reiss T 2021 Graphene Roadmap Briefs (No. 2): industrialization status and prospects 2020 *2D Mater.* **8** 022005

[8] Commissioning completion of the 4,000 metric tons per year graphene production capacity facility (available at: https://nanoxplore.ca/commissioning-completion-of-the-4000-metric-tons-per-year-graphene-production-capacity-facility/)

[9] The industrialization of graphene in China—the sixth element group opens a new plant (available at: www.azom.com/article.aspx?ArticleID=19751)
[10] FutureMarketsInc *The Graphene Market Report 2021* (available at: www.futuremarketsinc.com/category/all-reports/)
[11] Raghavan N, Thangavel S and Venugopal G 2017 A short review on preparation of graphene from waste and bioprecursors *Appl. Mater. Today* **7** 246–54
[12] Hussain A, Mehdi S M, Abbas N, Hussain M and Naqvi R A 2020 Synthesis of graphene from solid carbon sources: a focused review *Mater. Chem. Phys.* **248** 122924
[13] Fang Z *et al* 2020 Conversion of biological solid waste to graphene-containing biochar for water remediation: a critical review *Chem. Eng. J.* **390** 124611
[14] Kumar R, Singh R K and Singh D P 2016 Natural and waste hydrocarbon precursors for the synthesis of carbon based nanomaterials: graphene and CNTs *Renew. Sustain. Energy Rev.* **58** 976–1006
[15] Paredes J I and Villar-Rodil S 2016 Biomolecule-assisted exfoliation and dispersion of graphene and other two-dimensional materials: a review of recent progress and applications *Nanoscale* **8** 15389–413
[16] Geng Y, Wang S J and Kim J-K 2009 Preparation of graphite nanoplatelets and graphene sheets *J. Colloid Interface Sci.* **336** 592–8
[17] He P, Zhou C, Tian S, Sun J, Yang S, Ding G, Xie X and Jiang M 2015 Urea-assisted aqueous exfoliation of graphite for obtaining high-quality graphene *Chem. Commun.* **51** 4651–4
[18] Singh V V *et al* 2012 Greener electrochemical synthesis of high quality graphene nanosheets directly from pencil and its SPR sensing application *Adv. Funct. Mater.* **22** 2352–62
[19] Paredes J I, Villar-Rodil S, Fernández-Merino M J, Guardia L, Martínez-Alonso A and Tascón J M D 2011 Environmentally friendly approaches toward the mass production of processable graphene from graphite oxide *J. Mater. Chem.* **21** 298–306
[20] Liu J *et al* 2013 A green approach to the synthesis of high-quality graphene oxide flakes via electrochemical exfoliation of pencil core *RSC Adv.* **3** 11745–50
[21] Huang B, Liu Y, Guo Q, Fang Y, Titirici M-M, Wang X and Xie Z 2020 Porous carbon nanosheets from biological nucleobase precursor as efficient pH-independent oxygen reduction electrocatalyst *Carbon* **156** 179–86
[22] Torres F G, Troncoso O P, Rodriguez L and De-la-torre G E 2021 Sustainable synthesis, reduction and applications of graphene obtained from renewable resources *Sustain. Mater. Technol.* **29** e00310
[23] Azapagic A 2010 Assessing environmental sustainability: life cycle thinking and life cycle assessment *Sustainable Development in Practice* (West Sussex: John Wiley & Sons, Ltd) ed A Azapagic and S Perdan pp 56–80
[24] Guinée J B, Heijungs R, Huppes G, Zamagni A, Masoni P, Buonamici R, Ekvall T and Rydberg T 2011 Life cycle assessment: past, present, and future *Environ. Sci. Technol.* **45** 90–96
[25] Hauschild M Z *et al* 2013 Identifying best existing practice for characterization modeling in life cycle impact assessment *Int. J. Life Cycle Assess.* **18** 683–97
[26] Backes C *et al* 2020 Production and processing of graphene and related materials *2D Mater.* **7** 022001
[27] Tan C *et al* 2017 Recent advances in ultrathin two-dimensional nanomaterials *Chem. Rev.* **117** 6225–331
[28] Lee C, Wei X, Kysar J W and Hone J 2008 Measurement of the elastic properties and intrinsic strength of monolayer graphene *Science* **321** 385–8
[29] Geim A K and Novoselov K S 2007 The rise of graphene *Nat. Mater.* **6** 183–91
[30] Singh V, Joung D, Zhai L, Das S, Khondaker S I and Seal S 2011 Graphene based materials: past, present and future *Prog. Mater. Sci.* **56** 1178–271
[31] Pollard A J P, Keith R, Clifford C A and Legge E 2018 *Characterization of the Structure of Graphene* (available at: www.npl.co.uk/gpgs/graphene-structure-characterisation)
[32] Fadeel B *et al* 2018 Safety assessment of graphene-based materials: focus on human health and the environment *ACS Nano* **12** 10582–620
[33] Wick P *et al* 2014 Classification framework for graphene-based materials *Angew. Chem., Int. Ed.* **53** 7714–8
[34] Schroeder A, Levins C G, Cortez C, Langer R and Anderson D G 2010 Lipid-based nanotherapeutics for siRNA delivery *J. Intern. Med.* **267** 9–21
[35] Xia T, Kovochich M, Liong M, Zink J I and Nel A E 2008 Cationic polystyrene nanosphere toxicity depends on cell-specific endocytic and mitochondrial injury pathways *ACS Nano* **2** 85–96
[36] Hummers W S and Offeman R E 1958 Preparation of graphitic oxide *J. Am. Chem. Soc.* **80** 1339
[37] Ciesielski A and Samorì P 2014 Graphene via sonication assisted liquid-phase exfoliation *Chem. Soc. Rev.* **43** 381–98
[38] Niu L, Coleman J N, Zhang H, Shin H, Chhowalla M and Zheng Z 2016 Production of two-dimensional nanomaterials via liquid-based direct exfoliation *Small* **12** 272–93
[39] Hernandez Y *et al* 2008 High-yield production of graphene by liquid-phase exfoliation of graphite *Nat. Nanotechnol.* **3** 563–8
[40] Parvez K, Wu Z-S, Li R, Liu X, Graf R, Feng X and Müllen K 2014 Exfoliation of graphite into graphene in aqueous solutions of inorganic salts *J. Am. Chem. Soc.* **136** 6083–91
[41] Parvez K, Li R, Puniredd S R, Hernandez Y, Hinkel F, Wang S, Feng X and Müllen K 2013 Electrochemically exfoliated graphene as solution-processable, highly conductive electrodes for organic electronics *ACS Nano* **7** 3598–606
[42] Yang Y, Lu F, Zhou Z, Song W, Chen Q and Ji X 2013 Electrochemically cathodic exfoliation of graphene sheets in room temperature ionic liquids N-butyl, methylpyrrolidinium bis(trifluoromethylsulfonyl)imide and their electrochemical properties *Electrochim. Acta* **113** 9–16
[43] Morales G M, Schifani P, Ellis G, Ballesteros C, Martínez G, Barbero C and Salavagione H J 2011 High-quality few layer graphene produced by electrochemical intercalation and microwave-assisted expansion of graphite *Carbon* **49** 2809–16
[44] Abdelkader A M, Kinloch I A and Dryfe R A W 2014 Continuous electrochemical exfoliation of micrometer-sized graphene using synergistic ion intercalations and organic solvents *ACS Appl. Mater. Interfaces* **6** 1632–9
[45] Marcano D C, Kosynkin D V, Berlin J M, Sinitskii A, Sun Z, Slesarev A, Alemany L B, Lu W and Tour J M 2010 Improved synthesis of graphene oxide *ACS Nano* **4** 4806–14
[46] Dreyer D R, Park S, Bielawski C W and Ruoff R S 2010 The chemistry of graphene oxide *Chem. Soc. Rev.* **39** 228–40
[47] Zhu Y, Murali S, Cai W, Li X, Suk J W, Potts J R and Ruoff R S 2010 Graphene and graphene oxide: synthesis, properties, and applications *Adv. Mater.* **22** 3906–24
[48] Park S, An J, Potts J R, Velamakanni A, Murali S and Ruoff R S 2011 Hydrazine-reduction of graphite- and graphene oxide *Carbon* **49** 3019–23
[49] Stankovich S, Dikin D A, Piner R D, Kohlhaas K A, Kleinhammes A, Jia Y, Wu Y, Nguyen S T and Ruoff R S 2007 Synthesis of graphene-based nanosheets via chemical reduction of exfoliated graphite oxide *Carbon* **45** 1558–65
[50] Rowley-Neale S J, Randviir E P, Abo Dena A S and Banks C E 2018 An overview of recent applications of reduced graphene oxide as a basis of electroanalytical sensing platforms *Appl. Mater. Today* **10** 218–26
[51] Bonaccorso F, Bartolotta A, Coleman J N and Backes C 2016 2D-crystal-based functional inks *Adv. Mater.* **28** 6136–66

[52] Cai X, Luo Y, Liu B and Cheng H-M 2018 Preparation of 2D material dispersions and their applications *Chem. Soc. Rev.* **47** 6224–66
[53] Paton K R *et al* 2014 Scalable production of large quantities of defect-free few-layer graphene by shear exfoliation in liquids *Nat. Mater.* **13** 624–30
[54] Karagiannidis P G *et al* 2017 Microfluidization of graphite and formulation of graphene-based conductive inks *ACS Nano* **11** 2742–55
[55] León V, Quintana M, Herrero M A, Fierro J L G, Hoz A D L, Prato M and Vázquez E 2011 Few-layer graphenes from ball-milling of graphite with melamine *Chem. Commun.* **47** 10936–8
[56] Backes C *et al* 2016 Production of highly monolayer enriched dispersions of liquid-exfoliated nanosheets by liquid cascade centrifugation *ACS Nano* **10** 1589–601
[57] Bracamonte M V, Lacconi G I, Urreta S E and Foa Torres L E F 2014 On the nature of defects in liquid-phase exfoliated graphene *J. Phys. Chem.* C **118** 15455–9
[58] Backes C, Paton K R, Hanlon D, Yuan S, Katsnelson M I, Houston J, Smith R J, McCloskey D, Donegan J F and Coleman J N 2016 Spectroscopic metrics allow *in situ* measurement of mean size and thickness of liquid-exfoliated few-layer graphene nanosheets *Nanoscale* **8** 4311–23
[59] Munuera J M, Paredes J I, Villar-Rodil S, Castro-Muñiz A, Martínez-Alonso A and Tascón J M D 2018 High quality, low-oxidized graphene via anodic exfoliation with table salt as an efficient oxidation-preventing co-electrolyte for water/oil remediation and capacitive energy storage applications *Appl. Mater. Today* **11** 246–54
[60] Cooper A J, Wilson N R, Kinloch I A and Dryfe R A W 2014 Single stage electrochemical exfoliation method for the production of few-layer graphene via intercalation of tetraalkylammonium cations *Carbon* **66** 340–50
[61] Fusco L *et al* 2020 Graphene and other 2D materials: a multidisciplinary analysis to uncover the hidden potential as cancer theranostics *Theranostics* **10** 5435–88
[62] Backes C, Higgins T M, Kelly A, Boland C, Harvey A, Hanlon D and Coleman J N 2017 Guidelines for exfoliation, characterization and processing of layered materials produced by liquid exfoliation *Chem. Mater.* **29** 243–55
[63] Colombo L, Diebold A C, Casiraghi C, Kim M, Wallace R M and Venugopal A 2016 Archana characterization and metrology for graphene materials, structures, and devices *Metrology and Diagnostic Techniques for Nanoelectronics* ed Z Ma and D G Seiler (Boca Raton, FL: CRC Press) pp 759–848
[64] Zhang B and Su D S 2014 Transmission electron microscopy and the science of carbon nanomaterials *Small* **10** 222–9
[65] Read O, Shin Y, Hu C-X, Zarattini M, Boyes M, Just-Baringo X, Panigrahi A, Larrosa I and Casiraghi C 2021 Insights into the exfoliation mechanism of pyrene-assisted liquid phase exfoliation of graphene from lateral size-thickness characterisation *Carbon* **186** 550–9
[66] Jorio A, Saito R, Dresselhaus G and Dresselhaus M S 2011 *Raman Spectroscopy in Graphene Related Systems* (Hoboken, NJ: Wiley-VCH Verlag)
[67] Ferrari A C and Basko D M 2013 Raman spectroscopy as a versatile tool for studying the properties of graphene *Nat. Nanotechnol.* **8** 235–46
[68] Wu J-B, Lin M-L, Cong X, Liu H-N and Tan P-H 2018 Raman spectroscopy of graphene-based materials and its applications in related devices *Chem. Soc. Rev.* **47** 1822–73
[69] Cançado L G, Jorio A, Ferreira E H M, Stavale F, Achete C A, Capaz R B, Moutinho M V O, Lombardo A, Kulmala T S and Ferrari A C 2011 Quantifying defects in graphene via raman spectroscopy at different excitation energies *Nano Lett.* **11** 3190–6
[70] Eckmann A, Felten A, Verzhbitskiy I, Davey R and Casiraghi C 2013 Raman study on defective graphene: effect of the excitation energy, type, and amount of defects *Phys. Rev.* B **88** 035426
[71] Nagyte V *et al* 2020 Raman fingerprints of graphene produced by anodic electrochemical exfoliation *Nano Lett.* **20** 3411–9
[72] Baker S N and Baker G A 2010 Luminescent carbon nanodots: emergent nanolights *Angew. Chem., Int. Ed.* **49** 6726–44
[73] Liu F, Jang M-H, Ha H D, Kim J-H, Cho Y-H and Seo T S 2013 Facile synthetic method for pristine graphene quantum dots and graphene oxide quantum dots: origin of blue and green luminescence *Adv. Mater.* **25** 3657–62
[74] Srinivas G, Zhu Y, Piner R, Skipper N, Ellerby M and Ruoff R 2010 Synthesis of graphene-like nanosheets and their hydrogen adsorption capacity *Carbon* **48** 630–5
[75] Andrews E S *et al* 2009 *Guidelines for Social Life Cycle Assessment of Product* (Society of Environmental Toxicology and Chemistry (SETAC), United Nations Environmentl Programme (UNEP))
[76] ISO 2006 ISO 14040:2006 Environmental management—life cycle assessment—principles and framework (International Organization for Standardization)
[77] ISO 2006 ISO 14044:2006 Environmental management—life cycle assessment—requirements and guidelines (International Organization for Standardization)
[78] Curran M A 2014 Strengths and limitations of life cycle assessment *Background and Future Prospects in Life Cycle Assessment* ed W Klöpffer (Dordrecht: Springer) pp 189–206
[79] Müller L J, Kätelhön A, Bachmann M, Zimmermann A, Sternberg A and Bardow A 2020 A guideline for life cycle assessment of carbon capture and utilization *Front. Energy Res.* **8** 15
[80] Skone T J *et al* 2019 *Carbon Dioxide Utilization Life Cycle Analysis Guidance for the U.S. DOE Office of Fossil Energy* (National Energy Technology Laboratory)
[81] Hauschild M Z, Rosenbaum R K and Olsen S I 2018 *Life Cycle Assessment Theory and Practice* (Berlin: Springer)
[82] Zampori L, Saouter E, Schau E, Cristobal J, Castellani V and Sala S 2016 *Guide for Interpreting Life Cycle Assessment Result* (Joint Research Centre) (https://doi.org/10.2788/171315)
[83] Ecoinvent 2021 (available at: www.ecoinvent.org/home.html)
[84] Bauman H and Tillman A-M 2004 *The Hitch Hiker's Guide to LCA* (Sweden: Studentlitteratur AB)
[85] Balcombe P, Speirs J F, Brandon N P and Hawkes A D 2018 Methane emissions: choosing the right climate metric and time horizon *Environ. Sci.: Process. Impacts* **20** 1323–39
[86] EPA 2020 *Understanding Global Warming Potentials* (United States Environmental Protection Agency)
[87] CML CML-IA Characterisation Factors (available at: www.universiteitleiden.nl/en/research/research-output/science/cml-ia-characterisation-factors)
[88] NIPHE 2016 *ReCiPe 2016 v1.1* (National Institute for Public Health and the Environment)
[89] EC ILCD handbook (available at: https://eplca.jrc.ec.europa.eu/ilcdHandbook.html)
[90] EPA Tool for Reduction and Assessment of Chemicals and Other Environmental Impacts (TRACI)
[91] SimaPro (available at: www.simapro.co.uk/)
[92] Sphera (available at: www.gabi-software.com/uk-ireland/index/)
[93] OpenLCA (available at: www.openlca.org/)
[94] CCaLC2 (available at: www.ccalc.org.uk/)
[95] Kim D-Y, Nishiyama Y, Wada M and Kuga S 2001 Graphitization of highly crystalline cellulose *Carbon* **39** 1051–6
[96] Sevilla M and Fuertes A B 2010 Graphitic carbon nanostructures from cellulose *Chem. Phys. Lett.* **490** 63–68

[97] Yoo S, Chung C-C, Kelley S S and Park S 2018 Graphitization behavior of loblolly pine wood investigated by *in situ* high temperature x-ray diffraction *ACS Sustain. Chem. Eng.* **6** 9113–9
[98] Zhao H and Zhao T S 2013 Graphene sheets fabricated from disposable paper cups as a catalyst support material for fuel cells *J. Mater. Chem.* A **1** 183–7
[99] Adolfsson K H, Hassanzadeh S and Hakkarainen M 2015 Valorization of cellulose and waste paper to graphene oxide quantum dots *RSC Adv.* **5** 26550–8
[100] Xu D, Xie Y, Song Y-J and Deng W-Q 2015 A green and facile method toward synthesis of waste paper-derived 3D functional porous graphene via *in situ* activation of cobalt(ii) *J. Mater. Chem.* A **3** 16072–8
[101] Ye T-N, Feng W-J, Zhang B, Xu M, Lv L-B, Su J, Wei X, Wang K-X, Li X-H and Chen J-S 2015 Converting waste paper to multifunctional graphene-decorated carbon paper: from trash to treasure *J. Mater. Chem.* A **3** 13926–32
[102] Singu D C, Joseph B, Velmurugan V, Ravuri S and Grace A N 2017 Combustion synthesis of graphene from waste paper for high performance supercapacitor electrodes *Int. J. Nanosci.* **17** 1760023
[103] Xie F *et al* 2019 Unveiling the role of hydrothermal carbon dots as anodes in sodium-ion batteries with ultrahigh initial coulombic efficiency *J. Mater. Chem.* A **7** 27567–75
[104] Akhavan O, Bijanzad K and Mirsepah A 2014 Synthesis of graphene from natural and industrial carbonaceous wastes *RSC Adv.* **4** 20441–8
[105] Chyan Y, Ye R, Li Y, Singh S P, Arnusch C J and Tour J M 2018 Laser-induced graphene by multiple lasing: toward electronics on cloth, paper, and food *ACS Nano* **12** 2176–83
[106] Li J, Yan Q, Zhang X, Zhang J and Cai Z 2019 Efficient conversion of ligninwaste to high value bio-graphene oxide nanomaterials *Polymers* **11** 623
[107] Gomez-Martin A, Martinez-Fernandez J, Ruttert M, Winter M, Placke T and Ramirez-Rico J 2019 Porous graphene-like carbon from fast catalytic decomposition of biomass for energy storage applications *ACS Omega* **4** 21446–58
[108] Sun Z, Zheng M, Hu H, Dong H, Liang Y, Xiao Y, Lei B and Liu Y 2018 From biomass wastes to vertically aligned graphene nanosheet arrays: a catalyst-free synthetic strategy towards high-quality graphene for electrochemical energy storage *Chem. Eng. J.* **336** 550–61
[109] Sun L, Tian C, Li M, Meng X, Wang L, Wang R, Yin J and Fu H 2013 From coconut shell to porous graphene-like nanosheets for high-power supercapacitors *J. Mater. Chem.* A **1** 6462–70
[110] Tade R S and Patil P O 2020 Green synthesis of fluorescent graphene quantum dots and its application in selective curcumin detection *Curr. Appl. Phys.* **20** 1226–36
[111] Darminto, Asih R, Kurniasari, Baqiya M A, Mustofa S, Suasmoro, Kawamata T, Kato M, Watanabe I and Koike Y 2018 Enhanced magnetism by temperature induced defects in reduced graphene oxide prepared from coconut shells *IEEE Trans. Magn.* **54** 1600105
[112] Asih R, Yutomo E B, Ristiani D, Baqiya M A, Kawamata T, Kato M, Watanabe I and Koike Y 2019 Darminto, comparative study on magnetism of reduced graphene oxide (rGO) prepared from coconut shells and the commercial product *Mater. Sci. Forum* **966** 290–5
[113] Tamilselvi R, Ramesh M, Lekshmi G S, Bazaka O, Levchenko I, Bazaka K and Mandhakini M 2020 Graphene oxide—based supercapacitors from agricultural wastes: a step to mass production of highly efficient electrodes for electrical transportation systems *Renew. Energy* **151** 731–9
[114] Yadav K K, Singh H, Rana S, Sunaina, Sammi H, Nishanthi S T, Wadhwa R, Khan N and Jha M 2020 Utilization of waste coir fibre architecture to synthesize porous graphene oxide and their derivatives: an efficient energy storage material *J. Clean. Prod.* **276** 124240
[115] Salisu Nasir M Z H, Yusof N A and Zainal Z 2017 Oil palm waste-based precursors as a renewable and economical carbon sources for the preparation of reduced graphene oxide from graphene oxide *Nanomaterials* **7** 182
[116] Nurdin I, Fitri H R, Widiatmoko P, Devianto H and Prakoso T 2020 The effect of cationic CTAB surfactants on the performance of graphene electrode for supercapacitor *IOP Conf. Ser.: Mater. Sci. Eng.* **823** 012038
[117] Ray A K, Sahu R K, Rajinikanth V, Bapari H, Ghosh M and Paul P 2012 Preparation and characterization of graphene and Ni-decorated graphene using flower petals as the precursor material *Carbon* **50** 4123–9
[118] Lu X, Xiang K, Wang Y, Zhou W, Zhu Y, Chen W, Chen X, Chen H, Cheng H and Lu Z 2019 Selective preparation of graphene- and rope-like NanoCarbons from camellia wastes as high performance electrode materials for energy storage *J. Alloys Compd.* **811** 151616
[119] Pham H D, Mahale K, Hoang T M L, Mundree S G, Gomez-Romero P and Dubal D P 2020 Dual carbon potassium-ion capacitors: biomass-derived graphene-like carbon nanosheet cathodes *ACS Appl. Mater. Interfaces* **12** 48518–25
[120] Babu D B and Ramesha K 2019 Melamine assisted liquid exfoliation approach for the synthesis of nitrogen doped graphene-like carbon nano sheets from bio-waste bagasse material and its application towards high areal density Li-S batteries *Carbon* **144** 582–90
[121] Baweja H and Jeet K 2019 Economical and green synthesis of graphene and carbon quantum dots from agricultural waste *Mater. Res. Express* **6** 0850g8
[122] Hashmi A, Singh A K, Jain B and Singh A 2020 Muffle atmosphere promoted fabrication of graphene oxide nanoparticle by agricultural waste *Fullerenes Nanotubes Carbon Nanostruct.* **28** 1–10
[123] Zhao H, Cheng Y, Zhang Z, Zhang B, Pei C, Fan F and Ji G 2021 Biomass-derived graphene-like porous carbon nanosheets towards ultralight microwave absorption and excellent thermal infrared properties *Carbon* **173** 501–11
[124] Chen F, Yang J, Bai T, Long B and Zhou X 2016 Facile synthesis of few-layer graphene from biomass waste and its application in lithium ion batteries *J. Electroanal. Chem.* **768** 18–26
[125] Goswami S, Banerjee P, Datta S, Mukhopadhayay A and Das P 2017 Graphene oxide nanoplatelets synthesized with carbonized agro-waste biomass as green precursor and its application for the treatment of dye rich wastewater *Process. Saf. Environ. Prot.* **106** 163–72
[126] Ding J, Wang H, Li Z, Cui K, Karpuzov D, Tan X, Kohandehghan A and Mitlin D 2015 Peanut shell hybrid sodium ion capacitor with extreme energy–power rivals lithium ion capacitors *Energy Environ. Sci.* **8** 941–55
[127] Sha T, Liu J, Sun M, Li L, Bai J, Hu Z and Zhou M 2019 Green and low-cost synthesis of nitrogen-doped graphene-like mesoporous nanosheets from the biomass waste of okara for the amperometric detection of vitamin C in real samples *Talanta* **200** 300–6
[128] Choudhary R, Pandey O P and Brar L K 2021 High yield glucose assisted carbonization of soy flour for dye removal applications *Mater. Chem. Phys.* **260** 124174
[129] Suryawanshi A, Biswal M, Mhamane D, Gokhale R, Patil S, Guin D and Ogale S 2014 Large scale synthesis of graphene quantum dots (GQDs) from waste biomass and their use as an efficient and selective photoluminescence on–off–on probe for Ag+ ions *Nanoscale* **6** 11664–70
[130] Shams S S, Zhang L S, Hu R, Zhang R and Zhu J 2015 Synthesis of graphene from biomass: a green chemistry approach *Mater. Lett.* **161** 476–9
[131] Muramatsu H, Kim Y A, Yang K-S, Cruz-Silva R, Toda I, Yamada T, Terrones M, Endo M, Hayashi T and Saitoh H 2014 Rice husk-derived graphene with nano-sized domains and clean edges *Small* **10** 2766–70
[132] Wang H *et al* 2013 Interconnected carbon nanosheets derived from hemp for ultrafast supercapacitors with high energy *ACS Nano* **7** 5131–41

[133] Panahi-Kalamuei M, Amiri O and Salavati-Niasari M 2020 Green hydrothermal synthesis of high quality single and few layers graphene sheets by bread waste as precursor *J. Mater. Res. Technol.* **9** 2679–90
[134] Wang Z *et al* 2015 Microwave plasma-induced graphene-sheet fibers from waste coffee grounds *J. Mater. Chem.* A **3** 14545–9
[135] Sundriyal P and Bhattacharya S 2017 Polyaniline silver nanoparticle coffee waste extracted porous graphene oxide nanocomposite structures as novel electrode material for rechargeable batteries *Mater. Res. Express* **4** 035501
[136] Amir Faiz M S, Che Azurahanim C A, Yazid Y, Suriani A B and Siti Nurul Ain M J 2020 Preparation and characterization of graphene oxide from tea waste and it's photocatalytic application of TiO2/graphene nanocomposite *Mater. Res. Express* **7** 015613
[137] Abbas A, Tabish T A, Bull S J, Lim T M and Phan A N 2020 High yield synthesis of graphene quantum dots from biomass waste as a highly selective probe for Fe3+ sensing *Sci. Rep.* **10** 21262
[138] Tewari C, Tatrari G, Karakoti M, Pandey S, Pal M, Rana S, SanthiBhushan B, Melkani A B, Srivastava A and Sahoo N G 2019 A simple, eco-friendly and green approach to synthesis of blue photoluminescent potassium-doped graphene oxide from agriculture waste for bio-imaging applications *Mater. Sci. Eng.* C **104** 109970
[139] Li X-H, Kurasch S, Kaiser U and Antonietti M 2012 Synthesis of monolayer-patched graphene from glucose *Angew. Chem., Int. Ed.* **51** 9689–92
[140] Wang X *et al* 2013 Three-dimensional strutted graphene grown by substrate-free sugar blowing for high-power-density supercapacitors *Nat. Commun.* **4** 2905
[141] Zhang B, Song J, Yang G and Han B 2014 Large-scale production of high-quality graphene using glucose and ferric chloride *Chem. Sci.* **5** 4656–60
[142] Papaioannou N, Marinovic A, Yoshizawa N, Goode A E, Fay M, Khlobystov A, Titirici M-M and Sapelkin A 2018 Structure and solvents effects on the optical properties of sugar-derived carbon nanodots *Sci. Rep.* **8** 6559
[143] Yao M, Huang J, Deng Z, Jin W, Yuan Y, Nie J, Wang H, Du F and Zhang Y 2020 Transforming glucose into fluorescent graphene quantum dots via microwave radiation for sensitive detection of Al3+ ions based on aggregation-induced enhanced emission *Analyst* **145** 6981–6
[144] Pan F, Jin J, Fu X, Liu Q and Zhang J 2013 Advanced oxygen reduction electrocatalyst based on nitrogen-doped graphene derived from edible sugar and urea *ACS Appl. Mater. Interfaces* **5** 11108–14
[145] Poornima Parvathi V, Umadevi M and Bhaviya Raj R 2015 Improved waste water treatment by bio-synthesized graphene sand composite *J. Environ. Manage.* **162** 299–305
[146] Yassin M A, Mohamed I M A, Al-Mubaddel F S and Barakat N A M 2017 Effective and high performance graphene electrode for acidic electrolyte supercapacitors prepared from commercial sugar by one-pot procedure *Mater. Lett.* **201** 22–26
[147] Hou J, Cao C, Idrees F and Ma X 2015 Hierarchical porous nitrogen-doped carbon nanosheets derived from silk for ultrahigh-capacity battery anodes and supercapacitors *ACS Nano* **9** 2556–64
[148] Primo A, Atienzar P, Sanchez E, Delgado J M and García H 2012 From biomass wastes to large-area, high-quality, N-doped graphene: catalyst-free carbonization of chitosan coatings on arbitrary substrates *Chem. Commun.* **48** 9254–6
[149] Lavorato C, Primo A, Molinari R and Garcia H 2014 N-doped graphene derived from biomass as a visible-light photocatalyst for hydrogen generation from water/methanol mixtures *Chem. Eur. J.* **20** 187–94
[150] Zhang D-W *et al* 2018 Photoelectrochemical response of carbon dots (CDs) derived from chitosan and their use in electrochemical imaging *Mater. Horiz.* **5** 423–8
[151] Gao L, Zhang G, Cai J, Huang L, Zhou J and Zhang L 2020 Rationally exfoliating chitin into 2D hierarchical porous carbon nanosheets for high-rate energy storage *Nano Res.* **13** 1604–13
[152] Ling Z, Wang Z, Zhang M, Yu C, Wang G, Dong Y, Liu S, Wang Y and Qiu J 2016 Sustainable synthesis and assembly of biomass-derived B/N co-doped carbon nanosheets with ultrahigh aspect ratio for high-performance supercapacitors *Adv. Funct. Mater.* **26** 111–9
[153] Li H, Hu J, Meng Y, Su J and Wang X 2017 An investigation into the rapid removal of tetracycline using multilayered graphene-phase biochar derived from waste chicken feather *Sci. Total Environ.* **603–604** 39–48
[154] Pajarito B, Belamino A J, Calimbas R M and Gonzales J R 2020 Rizza mae calimbas and jillian rae gonzales, graphite nanoplatelets from waste chicken feathers *Materials* **13** 2109
[155] Bernardes A M, Espinosa D C R and Tenório J A S 2004 Recycling of batteries: a review of current processes and technologies *J. Power Sources* **130** 291–8
[156] Roy I, Sarkar G, Mondal S, Rana D, Bhattacharyya A, Saha N R, Adhikari A, Khastgir D, Chattopadhyay S and Chattopadhyay D 2016 Synthesis and characterization of graphene from waste dry cell battery for electronic applications *RSC Adv.* **6** 10557–64
[157] Rahmawati F, Prasasti B L W and Mudjijono M 2018 Graphene oxide from carbon rod waste *IOP Conf. Ser.: Mater. Sci. Eng.* **333** 012012
[158] Ambrosi A and Pumera M 2018 Exfoliation of layered materials using electrochemistry *Chem. Soc. Rev.* **47** 7213–24
[159] Bandi S, Ravuri S, Peshwe D R and Srivastav A K 2019 Graphene from discharged dry cell battery electrodes *J. Hazard. Mater.* **366** 358–69
[160] Prakoso B, Ma Y, Stephanie R, Hawari N H, Suendo V, Judawisastra H, Zong Y, Liu Z and Sumboja A 2020 Facile synthesis of battery waste-derived graphene for transparent and conductive film application by an electrochemical exfoliation method *RSC Adv.* **10** 10322–8
[161] Wang Y, Cao H, Chen L, Chen C, Duan X, Xie Y, Song W, Sun H and Wang S 2018 Tailored synthesis of active reduced graphene oxides from waste graphite: structural defects and pollutant-dependent reactive radicals in aqueous organics decontamination *Appl. Catal.* B **229** 71–80
[162] Li B, Wu C, Xu J, Hu D, Zhang T, Fang X and Tong J 2020 One-pot redox synthesis of graphene from waste graphite of spent lithium ion batteries with peracetic acid assistance *Mater. Chem. Phys.* **241** 122397
[163] Yu J, Lin M, Tan Q and Li J 2021 High-value utilization of graphite electrodes in spent lithium-ion batteries: from 3D waste graphite to 2D graphene oxide *J. Hazard. Mater.* **401** 123715
[164] Zhang Y, Song N, He J, Chen R and Li X 2019 Lithiation-aided conversion of end-of-life lithium-ion battery anodes to high-quality graphene and graphene oxide *Nano Lett.* **19** 512–9
[165] Wong C H A, Sofer Z, Kubešová M, Kučera J, Matějková S and Pumera M 2014 Synthetic routes contaminate graphene materials with a whole spectrum of unanticipated metallic elements *Proc. Natl Acad. Sci.* **111** 13774–9
[166] González-Barriuso M, Yedra A, Mantilla P and Manteca-Martínez C 2015 Synthesis and characterisation of reduced graphene oxide from graphite waste and HOPG *Mater. Res. Innov.* **19** 192–5
[167] Barbakadze N G, Tsitsishvili V G, Korkia T V, Amiridze Z G, Jalabadze N V and Chedia R V 2018 Synthesis of graphene oxide and reduced graphene oxide from industrial graphite foil wastes *European Chem.l Bull.* **7** 329–33 (available at: www.eurchembull.com/archives/)
[168] Eny Kusrini A S, Usman A, Khalil M and Degirmenci V 2019 Synthesis and characterization of graphite oxide,

graphene oxide, and reduced graphene oxide from graphite waste using modified hummers' method and zinc as reducing agent *Int. J. Technol.* **10** 1093–104
[169] Ding S, Sun S, Xu H, Yang B, Liu Y, Wang H, Chen D and Zhang R 2019 Preparation and adsorption property of graphene oxide by using waste graphite from diamond synthesis industry *Mater. Chem. Phys.* **221** 47–57
[170] Tian Z, Cao K, Bai S, He G and Li J 2019 One-pot transformation of waste toner powder into 3D graphene oxide hydrogel *ACS Sustain. Chem. Eng.* **7** 496–501
[171] Jlassi K, Mallick S, Eribi A, Chehimi M M, Ahmad Z, Touati F and Krupa I 2021 Facile preparation of N-S co-doped graphene quantum dots (GQDs) from graphite waste for efficient humidity sensing *Sens. Actuators* B **328** 129058
[172] Udhaya Sankar G, Ganesa Moorthy C and RajKumar G 2018 Synthesizing graphene from waste mosquito repellent graphite rod by using electrochemical exfoliation for battery/supercapacitor applications *Energy Sources* A **40** 1209–14
[173] Zhou Q, Zhao Z, Zhang Y, Meng B, Zhou A and Qiu J 2012 Graphene sheets from graphitized anthracite coal: preparation, decoration, and application *Energy Fuels* **26** 5186–92
[174] Ye R *et al* 2013 Coal as an abundant source of graphene quantum dots *Nat. Commun.* **4** 2943
[175] Lawagon C P, Faungnawakij K, Srinives S, Thongratkaew S, Chaipojjana K, Smuthkochorn A, Srisrattha P and Charinpanitkul T 2020 Sulfonated graphene oxide from petrochemical waste oil for efficient conversion of fructose into levulinic acid *Catal. Today* **375** 197–203
[176] Kumar Sahoo S, Kumar Sahoo J, Kumar Panigrahi G, Kumar Pattanayak D, Sundar Rout A and Lenka A 2020 Preparation of graphene oxide from bio-soot wastes: as an efficient adsorbent for highly noxious Congo red dye *FlatChem* **24** 100198
[177] Yang W, Li R, Jiang B, Wang T, Hou L, Li Z, Liu Z, Yang F and Li Y 2020 Production of hierarchical porous carbon nanosheets from cheap petroleum asphalt toward lightweight and high-performance electromagnetic wave absorbents *Carbon* **166** 218–26
[178] Luong D X *et al* 2020 Gram-scale bottom-up flash graphene synthesis *Nature* **577** 647–51
[179] Algozeeb W A, Savas P E, Luong D X, Chen W, Kittrell C, Bhat M, Shahsavari R and Tour J M 2020 Flash graphene from plastic waste *ACS Nano* **14** 15595–604
[180] Gong J, Liu J, Wen X, Jiang Z, Chen X, Mijowska E and Tang T 2014 Upcycling waste polypropylene into graphene flakes on organically modified montmorillonite *Ind. Eng. Chem. Res.* **53** 4173–81
[181] Pandey S, Karakoti M, Dhali S, Karki N, SanthiBhushan B, Tewari C, Rana S, Srivastava A, Melkani A B and Sahoo N G 2019 Bulk synthesis of graphene nanosheets from plastic waste: an invincible method of solid waste management for better tomorrow *Waste Manage.* **88** 48–55
[182] El Essawy N A, Ali S M, Farag H A, Konsowa A H, Elnouby M and Hamad H A 2017 Green synthesis of graphene from recycled PET bottle wastes for use in the adsorption of dyes in aqueous solution *Ecotoxicol. Environ. Saf.* **145** 57–68
[183] Ko S, Kwon Y J, Lee J U and Jeon Y-P 2020 Preparation of synthetic graphite from waste PET plastic *J. Ind. Eng. Chem.* **83** 449–58
[184] Stanford M G, Yang K, Chyan Y, Kittrell C and Tour J M 2019 Laser-induced graphene for flexible and embeddable gas sensors *ACS Nano* **13** 3474–82
[185] Huang H, Peng L, Fang W, Cai S, Chu X, Liu Y, Gao W, Xu Z and Gao C 2020 A polyimide-pyrolyzed carbon waste approach for the scalable and controlled electrochemical preparation of size-tunable graphene *Nanoscale* **12** 11971–8
[186] Nguyen D D, Hsieh P-Y, Tsai M-T, Lee C-Y, Tai N-H, To B D, Vu D T and Hsu C C 2017 Hollow few-layer graphene-based structures from parafilm waste for flexible transparent supercapacitors and oil spill cleanup *ACS Appl. Mater. Interfaces* **9** 40645–54
[187] Wang C, Li D, Zhai T, Wang H, Sun Q and Li H 2019 Direct conversion of waste tires into three-dimensional graphene *Energy Storage Mater.* **23** 499–507
[188] Arvidsson R, Kushnir D, Sandén B A and Molander S 2014 Prospective life cycle assessment of graphene production by ultrasonication and chemical reduction *Environ. Sci. Technol.* **48** 4529–36
[189] Pizza A, Metz R, Hassanzadeh M and Bantignies J-L 2014 Life cycle assessment of nanocomposites made of thermally conductive graphite nanoplatelets *Int. J. Life Cycle Assess.* **19** 1226–37
[190] Sun L, Yu H and Fugetsu B 2012 Graphene oxide adsorption enhanced by *in situ* reduction with sodium hydrosulfite to remove acridine orange from aqueous solution *J. Hazard. Mater.* **203–204** 101–10
[191] Chen W, Yan L and Bangal P R 2010 Preparation of graphene by the rapid and mild thermal reduction of graphene oxide induced by microwaves *Carbon* **48** 1146–52
[192] Pham T A, Kim J S, Kim J S and Jeong Y T 2011 One-step reduction of graphene oxide with l-glutathione *Colloids Surf.* A **384** 543–8
[193] Brodie B C XIII 1859 On the atomic weight of graphite *Phil. Trans. R. Soc.* **149** 249–59
[194] Staudenmaier L 1898 Verfahren zur Darstellung der Graphitsäure *Berichte der deutschen chemischen Gesellschaft* **31** 1481–7
[195] Zhang S *et al* 2020 Sustainable production of value-added carbon nanomaterials from biomass pyrolysis *Nat. Sustain.* **3** 753–60
[196] Ampah A D, Pagone E and Salonitis K 2019 *Life Cycle Assessment of Graphene as Heating Element* (Singapore: Springer) pp 283–97
[197] Arvidsson R, Kushnir D, Molander S and Sandén B A 2016 Energy and resource use assessment of graphene as a substitute for indium tin oxide in transparent electrodes *J. Clean. Prod.* **132** 289–97
[198] Arvidsson R and Molander S 2017 Prospective life cycle assessment of epitaxial graphene production at different manufacturing scales and maturity *J. Ind. Ecol.* **21** 1153–64
[199] Khanam P N, Popelka A, Alejji M and AlMaadeed M A 2017 Biotechnological production process and life cycle assessment of graphene *J. Nanomater.* **2017** 5671584
[200] Cossutta M, McKechnie J and Pickering S J 2017 A comparative LCA of different graphene production routes *Green Chem.* **19** 5874–84
[201] Serrano-Luján L, Víctor-Román S, Toledo C, Sanahuja-Parejo O, Mansour A E, Abad J, Amassian A, Benito A M, Maser W K and Urbina A 2019 Environmental impact of the production of graphene oxide and reduced graphene oxide *SN Appl. Sci.* **1** 179
[202] Scott R P and Cullen A C 2016 Reducing the life cycle environmental impacts of kesterite solar photovoltaics: comparing carbon and molybdenum back contact options *Int. J. Life Cycle Assess.* **21** 29–43
[203] Beloin-Saint-Pierre D and Hischier R 2021 Towards a more environmentally sustainable production of graphene-based materials *Int. J. Life Cycle Assess.* **26** 327–43